Method development in analysis of cerium dioxide and titanium dioxide nanoparticles with sp-ICP-MS

INSTITUTE OF MARINE RESEARCH

Master thesis in chemistry

By

Mathias Simonsen

Department of Chemistry, University of Bergen

Institute of Marine Research

August 2022

Preface

This master thesis in chemistry is written in collaboration with the Chemistry Department at University of Bergen (UoB) and the Institute of Marine Research (IMR). All work related to analysis with sp-ICP-MS was done at IMR, while the analysis by electron microscopy was done at the Department of Earth Science at UoB.

First and foremost, I want to thank my supervisors André Marcel Bienfait (IMR) and Kristine Spildo (UoB) for excellent guidance throughout the project. Furthermore, I would like to thank Irene Heggstad at ELMIlab (UoB) for help during the preparation and conducting of electron microscopy analysis. Thanks to Berit Solli and Vivian Krakeli (IMR) for being a resource at the laboratory when meeting practical or instrumental obstacles. A special thanks to PhD student Are Sæle Bruvold (IMR) for your time, help and ideas. Also, thanks to Stig Valdersnes (IMR), fellow student Thea Bakken, and the rest of the nano group for at IMR for the warm welcome and good discussions.

A final thanks to my wife, kids, family, friends, and fellow students for your encouragement.

- Mathias

Abstract

In the past decades, the supply and demand for target specific nanoparticles (NPs) has increased explosively as the nanoscience has continued to develop and emerge with new ways to utilize them in a wide variety of different fields. The understanding of the consequential environmental impact is lesser known, thus there is a need for a methodology to determine the type and content of NPs in biological samples. This thesis focuses on the use of single particle inductively coupled mass spectrometry (sp-ICP-MS) to analyze cerium(IV) oxide (CeO_2) and titanium(IV) oxide (TiO_2) in samples of mussel and cod fillet, respectively. Electron microscopy (EM) has been used as a complimentary technique.

During the project, CeO_2 30-50 nm NPs and TiO_2 <150 nm NPs have been analyzed both with and without biological matrices. The method in this thesis is based on a validation report made by staff at IMR for the spike and recovery analysis of Au NPs in mussels. Au NPs were also included in this thesis, to generate basis of comparison as well as for calibrating the instrument. Results showed that the measured concentrations of NPs detected for both CeO_2 and TiO_2 stock suspensions were lower than expected but could be explained by the small and undetectable sizes of many of the particles. The presence of natural nanoparticles complicated the process of determining the recovery; the concentration of TiO_2 in mussels was found to be too high, making it impossible to perform spike-recovery analysis. The challenge of working with highly polydisperse NPs with sizes near the detection limit is subdued by developing a method to refine the size distributions of the NPs, making them both larger and more monodisperse. The stability of the refined NPs is checked by storing them for 20-45 days before reanalyzing them. The refined NPs were also analyzed in biological matrices, and showed improvement compared to the unrefined NPs when it comes to robustness and reproducibility. The use of EM confirmed the size and shape of Au NPs and confirmed the sp-ICP-MS results for CeO_2 NPs to a large degree. EM analysis of TiO_2 NPs were attempted but did not give satisfactory results.

Abbreviations

ANP:	Anthropogenic nanoparticles
CPS:	Counts per second
CRM:	Certified reference material
EM:	Electron microscopy
EMP:	Engineered nanoparticle
ICP-MS:	Inductively coupled plasma mass spectrometry
LOD:	Limit of detection
LOQ:	Limit of quantification
m/z:	Mass to charge ratio
NNP:	Natural nanoparticle
NE:	Transport efficiency
NP:	Nanoparticle
PDT:	Particle detection threshold
ROS:	Reactive oxygen species
RSD:	Relative standard deviation
SD:	Standard deviation
SEM:	Scanning electron microscopy
sp-ICP-MS:	Single particle inductively couple plasma mass spectrometry

Table of contents

Preface 2

Abstract 3

Abbreviations 4

1. Introduction 7

1.1 Background 7

1.2 Objective 8

2. Theory 9

2.1 Definition of nanoparticles 9

2.1.1 Occurrence, Properties, and applications of nanoparticles 9

2.1.2 Toxicity of nanoparticles 10

2.2 Analytical techniques 10

2.2.1 Inductively coupled mass spectrometry 10

2.2.2 Single particle inductively coupled mass spectrometry 13

2.2.3 Sp-ICP-MS Equations 16

2.2.4 Scanning electron microscopy 18

2.3 Mathematical Equations 19

3. Experimental 21

3.1 Materials and instruments 21

3.2 Preparation of biological samples 22

3.3 Enzymatic digestion 23

3.4 Refinement process of CeO_2 NPs and TiO_2 NPs 25

3.4.1 Refinement of CeO_2 NPs 25

3.4.2 Refinement of TiO_2 NPs 26

3.5 sp-ICP-MS analysis 27

3.5.1 Dilution and analysis of Au 60 nm NPs. 27

3.5.2 Dilution and analysis of refined and unrefined cerium dioxide 30-50 nm NPs 28

3.5.3 Dilution and analysis of refined and unrefined Titanium dioxide <150 nm NPs 29

3.5.4 Dilution of ionic standards 30
3.6 Processing of data from sp-ICP-MS analysis. 30
3.7 Scanning electron microscopy 31
4. Results 32
4.1 sp-ICP-MS 32
4.1.1 Au 60 nm nanoparticles 32
4.1.2 Cerium dioxide 30-50 nm nanoparticles 34
4.1.3 Refined cerium dioxide nanoparticles 35
4.1.4 Titanium dioxide < 150 nm nanoparticles 41
4.1.5 Centrifuged titanium dioxide nanoparticles 41
4.2 Scanning Electron Microscopy (SEM) 48
4.2.1 Gold 60 nm nanoparticles 48
4.2.2 Cerium dioxide nanoparticles 50
4.2.3 Titanium dioxide nanoparticles 51
5. Discussion 53
5.1 Au 60 nm nanoparticles 53
5.2 Work-up and analysis of CeO_2 nanoparticles 53
5.2.1 Unrefined CeO_2 30-50 nm nanoparticles 53
5.2.2 Refined CeO_2 nanoparticles 54
5.3 Work-up and analysis of TiO_2 nanoparticles 55
5.3.1 Unrefined TiO_2 <150nm nanoparticles 55
5.3.2 Refined TiO_2 nanoparticles 56
6. Conclusion 58
7. Further research 58
8. References 58
9. Attachments 61

1. Introduction

1.1 Background

The use of nanoparticles today is extensive and has been rapidly increasing for the past two decades and is expected to continuously do so in the future[1]. The global production of engineered nanoparticles (ENPs) was in 2010 estimated to 2.68 – 3.18 million tons and has increased by 25% every year since then. The global nanotechnology market is expected to exceed 125 billion US dollars by 2024 [2]. NPs are used for its optical, physical, electrical and/or chemical properties, and the industrial applications are many. NPs are used in agriculture, food, cosmetics, electronics, and medicine to name a few. Recent years, the widespread use of NPs has led to an increasing concern for the potential impact and hazard on the environment and on our own health [3]. National and global regulators such as the FDA, EU, and OECD calls for more research and evidence on the matter.

The study of the environmental has proven[4] to be difficult due to the diverse nature of nanoparticles. Properties of NPs change by size, concentration, PH and more, which makes it difficult to generalize their risks. Another problem is the lack of methods to detect and analyze NPs in natural samples. Existing analyzing methods such as EM and DLS can measure NPs but requires a concentration far greater than what can be extracted from natural samples. Single particle inductively coupled plasma mass spectrometry (sp-ICP-MS) is a promising technique in the analysis of NPs in natural samples as it can detect and measure the number and content of NPs in the ppb-scale. The instrument can also calculate the size of the NPs if the elemental composition and density is known. Sp-ICP-MS also gives information of the FullQuant concentration, which includes both the particulate concentration and the concentration of dissolved analyte in the medium. The Institute of Marine research (IMR) has already made a validation report on the determination of Au NPs in mussels, and this thesis explores the possibility of using the validated method of CeO_2 and TiO_2 NPs, and if it can be applied to cod fillet as the biological matrix as well as mussels. Sp-ICP-MS is still considered a novel method. The lack of certified standard materials (CRMs) makes it difficult to generate standard methods. sp-ICP-MS is also subjected to human bias, as the placement of the particle detection threshold (PDT) is either manually adjusted or auto fixed by untrustworthy algorithms. This challenge is attempted subdued by refining the size distribution of the NPs to a higher median size, making the placement of the (PDT) more intuitive.

1.2 Objective

In this thesis, the main objective is to develop methods to determine the presence and contents of cerium oxide NPs and titanium oxide NPs in marine samples with sp-ICP-MS. The methods are developed by adapting and adjusting a preexisting method for determination of Au NPs in mussels by the Institute of Marine Research (IMR) [5]. Firstly, the sensitivity, and the ability to detect the particles without any matrices is assessed. The next step is to attempt to extract CeO_2 and TiO_2 NPs from spiked samples of mussels or cod. In addition, the well-known analytical challenge in nanoscience due to the lack of certified reference materials (CRMs) is met by performing a refinement procedure on stock dispersions of CeO_2 and TiO_2 NPs to alter the size distribution of the particles. Another objective is to verify the sp-ICP-MS results by electron microscopy (EM) analysis.

2. Theory

2.1 Definition of nanoparticles

The task of finding the right definition of NPs or nanomaterials is a topic of discussion, as there is no straight-forward way to do it. Nevertheless, as the demand, production and use of purpose specific nanoparticles are constantly increasing, policymakers need a legally and scientifically precise definition to be able to regulate the use and production of NPs. A nanomaterial is today defined by EU as a material where at least 50% or more of its constituent particles are between 1-100 nm in at least one external dimension [6].

2.1.1 Occurrence, Properties, and applications of nanoparticles

NPs in the environment can either be of natural or anthropogenic origin. Natural nanoparticles (NNPs) can be generated from a numerous different biological, physical, or chemical processes. Dust storms, wildfires, bio-chemical eroding of minerals in the soil are some examples [7]. Anthropogenic nanoparticles (ANPs) are a result of human activity and can either be incidental or engineered. As the name suggests, incidental NPs are not manufactured, but rather occur as waste or by-product. There are many sources of incidental NPs, such as waste from mining, combustion reactions, welding and more. Engineered nanoparticles (ENPs) are NPs that are intentionally manufactured with specific beneficial properties.

When materials are reduced to the nanoscale, the physio-chemical properties differ substantially from the same materials in bulk form. The key difference between bulk materials and nanomaterials is best described by the surface to volume-ratio; as the size of a particle decreases, a larger portion of the atoms in the particle are located at the surface. For example, a 100 nm particle will have approximately 1% of its atoms on the surface, at 10 nm 20% of its atoms and a 3 nm particle will have about 50% of its particle located at the surface [8]. Thus, a given mass of a material in the nano-range will be considerably more reactive than the same mass of the material in bulk-form. The reason for this dramatic change in reactivity comes from two types of fundamental effects: (a) The surface effect arises from the fact that atoms on the surface differ significantly from the atoms on the inside. The exterior atoms have fewer neighboring atoms and will possess more unfulfilled orbitals [9] leading to an increase in free energy, reactivity, and mobility. (b): Quantum effects becomes significant as the number of

atoms in a particle decreases below a critical limit specified for different materials [10], leading to an impact on the magnetic, optical, and electric properties of the material.

2.1.2 Toxicity of nanoparticles

While the progress and development of nanomaterials with positive impact has been formidable the past decades, the concern for potential health and environment threats are beginning to emerge. There are mainly three ways for nanoparticles to enter the body; through the skin, via inhaling or gastro-intestinal uptake. the latter two are generally of more concern as the absorption through the skin is limited due to the well-protective structure of skin with multiple layers of cells and tissue. After uptake, some nanoparticles may enter the bloodstream, thereby induce risk to the lymphatic system as well as other tissues and organs [11]. The generation of reactive oxygen species (ROS) is suggested as an important part of nanotoxicology. Overproduction of ROS can cause oxidative stress, inhibiting cells to maintain their redox-regulated functions [12], which can cause DNA damage [13], cell signaling errors [14], and cancer [15].

Compared to non-nano chemical toxicants, toxicological investigation of NPs is a much more complex matter, as the biochemical effect is dependent on its elemental composition, size, shape, agglomeration state, PH, and more. These factors affect the degree of cellular uptake, protein binding abilities, and tissue damage [16]. For instance, the production of ROS is shown to correlate with the size of TiO_2 particles [17]. The generation of ROS are similar when comparing exposure to NPs below 10 nm and above 30 nm, but dramatically increasing from 10 to 30 nm which indicates a biologically active size span between 10 – 30 nm.

2.2 Analytical techniques

2.2.1 Inductively coupled mass spectrometry

Single particle inductively coupled mass spectrometry (sp-ICP-MS) is based on the principles conventional ICP-MS, an important analytical tool for trace level analysis at extremely low concentrations. The technique has been developed over the past 40 years and is today considered favorable over other alternatives such as flame photometry and flame atomic absorption due to its multi-element capabilities combined with short analysis time, allowing

for a high sample throughput in the laboratory [18]. ICP-MS also has a wide dynamic range, from the lower ng/L region for qualitative assurance to the higher mg/L region for quantitative analysis. The major instrumental components are illustrated in **Figure** 2-1.

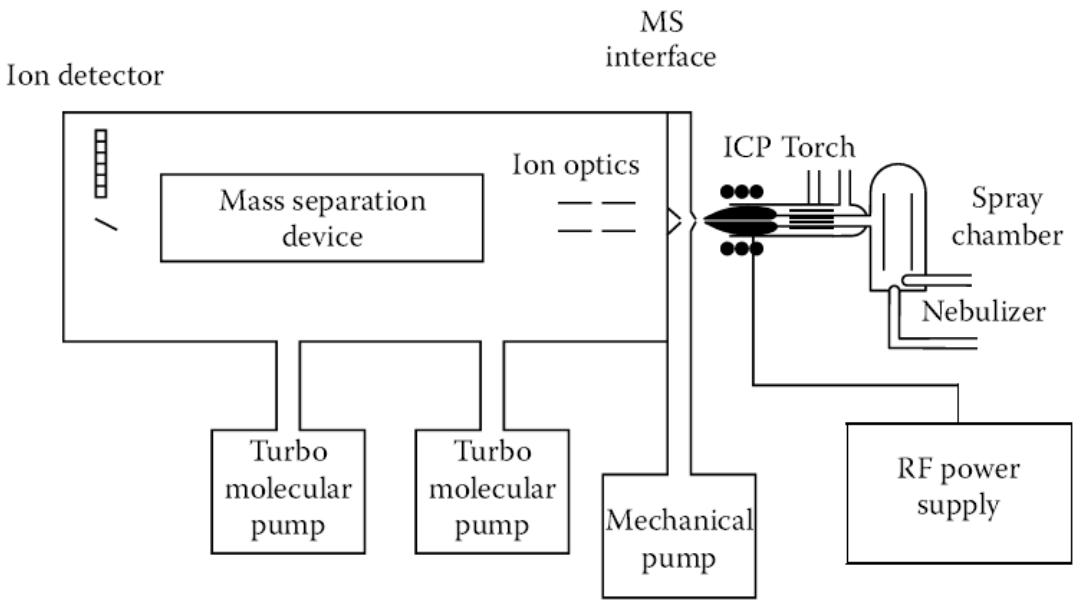

Figure 2-1: Main components of an ICP-MS instrument

ICP-MS is designed to handle liquid samples, but solid samples can be analyzed directly by using newer adaptations such as laser ablation or electrochemical vaporization[19]. This thesis focuses on liquid sample introduction. Before entering the ICP, the diluted sample is delivered to a pneumatic nebulizer which uses an argon gas flow to create an aerosol. The aerosol droplets then move on to a spray chamber, where the largest droplets (>10 μm) are filtered out. Only about 1-5% of the aerosol passes through the spray chamber. This serves an important function as the plasma is inefficient at dissociating larger droplets. The plasma is generated by s device usually referred to as the quartz-torch, which consists of three concentric quartz tubes. The innermost tube is called the injector and contains the aerosol sample in a stream of argon gas, called nebulizer gas, which delivers the sample to the plasma. The plasma gas (usually argon), used to form the plasma, passes through the outermost tube. A copper induction coil is surrounding the end of the torch and is connected to a radio frequency (RF) generator. The RF coil system induces an oscillating electromagnetic field of alternating current in the torch. A high-voltage spark is applied, causing a fraction of the argon atoms to be ionized, generating free electrons and ions. The ions and electrons are accelerated by the electromagnetic field.

This leads to new collisions between ions and argon atoms which subsequently generates more ions and electrons. The temperature increases with the propagation of charged particles and can reach as high as 10.000 K, depending on the instrument. When reaching the plasma, the small sample droplets generated by the nebulizer are desolvated, atomized and ultimately ionized to singly charged positive ions. The ions are then transported to the interface, which holds two nickel or platinum cones. The ions are guided through a small opening of about 1 mm of the sample cone into the area between the cones where the pressure is reduced drastically from atmospheric pressure in the plasma to about 150-300 Pa. The low pressure in the interface region generates a so-called free jet by causing a supersonic expansion [20] and is maintained by a mechanical pump. The ions are extracted into the main chamber through an even smaller opening of about 0.45 mm on the skimmer cone. The main chamber operates under high vacuum ($7x10^{-5}$– $1x10^{-3}$ Pa) generated by a turbomolecular pump. At this pressure, the ion beam can be guided by a set of electrostatic lenses, referred to as the ion optics. The ion optics main task is to guide the ion beam toward the mass analyzer, as well as preventing neutral species such as photons and non-ionized matrix components from reaching the mass detector, keeping photon-based noise and signal instability at a minimum. The ion optics design varies between manufacturers. In the Agilent instrument used in this project, photons are stopped by using an omega-lens (the name comes from its resemblance of the Greek letter Ω) which causes a slight shift in the direction of the ion beam.

After the ions have transited through the ion optics, they enter the mass analyzer. Different kinds of mass analyzers are being used in ICP-MS systems, but the far most common type is a quadrupole mass analyzer. A quadrupole is a mass filter consisting of four 15-20 cm long cylindrical or hyperbolic metal rods placed parallel to each other. As the stream of ions enters the quadrupole, the ions are separated based on their m/z ratio by applying oscillating radio frequency (RF) alternating current (AC) and direct current (DC) to the rods. This generates a time varying electric field in the center of the rods and can be adjusted to target specific ions with known m/z ratio, resulting in stable ion flight trajectories for these ions. An unstable flight trajectory will result in collisions with the rods.

The use of tandem mass spectrometry, sometimes referred to as MS/MS, with triple quadrupole instruments is a relatively new but increasingly used development in ICP-MS, which will be utilized for the analysis of TiO_2 NPs in this project. Instruments capable to conduct MS/MS analysis are equipped with an extra quadrupole placed upstream, prior to the standard

quadrupole mass analyzer. This quadrupole works as a preliminary mass filter, allowing only certain ionic species to enter the reaction cell. In the case of titanium, analysis of the most abundant isomer $^{48}Ti^{+}$ is subjected to isobaric interferences from multiple isobaric elements and polyatomic ions, such as $^{48}Ca^{+}$, $^{31}P^{17}O^{+}$, and more. By using the first quadrupole to only allow ions with *m/z* 48 to pass through to the reaction cell, a controlled reaction between the ions and a reaction gas consisting of O_2 and H_2 can take place. In the reaction cell, titanium will bind with oxygen, forming the ion $^{48}Ti^{16}O^{+}$ with *m/z* 64, which can be set as the target value in the last quadrupole. This is referred to as the mass-shift method. Another way to utilize the triple quadrupole instrument is called the "on-mass" method and works by eliminating isobaric ions in the reaction cell. As an example, $^{28}Si^{+}$ is interfered by $^{14}N_2^{+}$. By using H_2 as a reaction gas, $^{14}N_2^{+}$ will form $^{14}N_2H^{+}$ while $^{28}Si^{+}$ will not undergo any reaction, and will pass through the last quadrupole, while nitrogen species are filtered out.

2.2.2 Single particle inductively coupled mass spectrometry

The most important difference between conventional ICP-MS and sp-ICP-MS is shown in **Figure** 2-2. Completely dissolved analyte in the sample matrix results in a continuous stream of ions passing through to the mass analyzer, creating a constant signal shown in the top right corner of the Figure. When the analyte is confined to nanoparticles in a suspension, the ionization of a nanoparticle will produce a cluster of ions. The clusters will reach the mass

analyzer one by one, preferably, and give rise to one peak each. Correct dilution is crucial. In the case of too high concentration, overlap signals of two or more NPs will be interpreted as one large particle in the software. Too few particles detected will result in poor statistics and should be avoided. The intensity of the peak is related to the mass of the particle, and the frequency of peaks is related to the number of particles in the suspension. The mass of the NPs can be used to calculate the size of the NPs if the elemental composition and density of the particles are known. The MH-software assumes spherical shape in all its calculations [21].

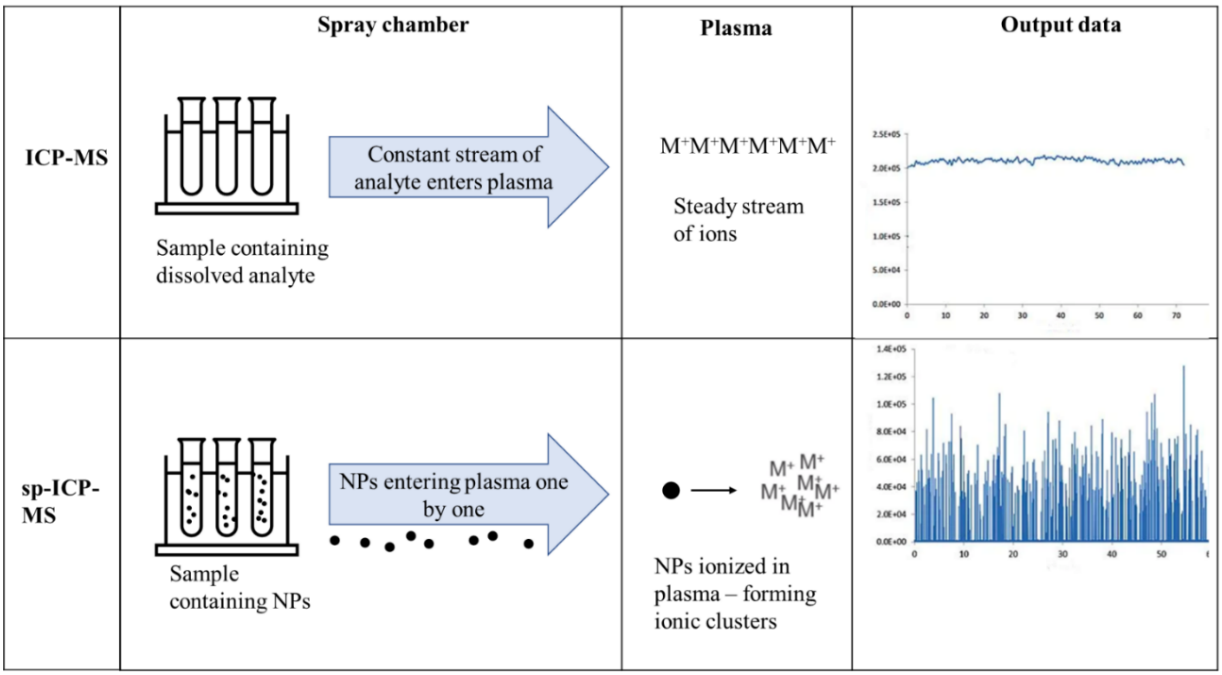

Figure 2-2: Main difference in the generation of raw signals between conventional ICP-MS and sp-ICP-MS

A typical signal from one NP ion cluster last for about 200-500 µs [22], and with newer instruments capable of analyzing with dwell times in the microsecond scale, multiple signals can be generated from a single NP, as shown in **Figure** 2-3 A. The signal background stems from dissolved analyte, electronic noise from the instrument, and potential sources of isobaric interferences. A time-resolved raw signal plot as shown in **Figure** 2-3 B and is collected if the instrument manages to detect multiple peaks over a background generated by NP signals over a period. This is converted into a histogram where the frequency of specific intensities gives the particle size distribution of the detected NPs. **Figure** 2-3C shows an example of an optimal distribution of Au NPs, where the NP signals is completely separated from the background. A particle detection threshold (PDT), or detection limit is then set, either manually or automatically. If set manually, the most common practice is to place the PDT based on visual interpretation of the plot [23]. In many cases, especially in natural samples, this is not achievable, as the NP signals often overlaps with the background. This causes issues in determining the correct placement of the PDT and is subjected to high variability and low degree of reproducibility and robustness, as it is up to either a novel software or individual opinions to decide placement of the PDT.

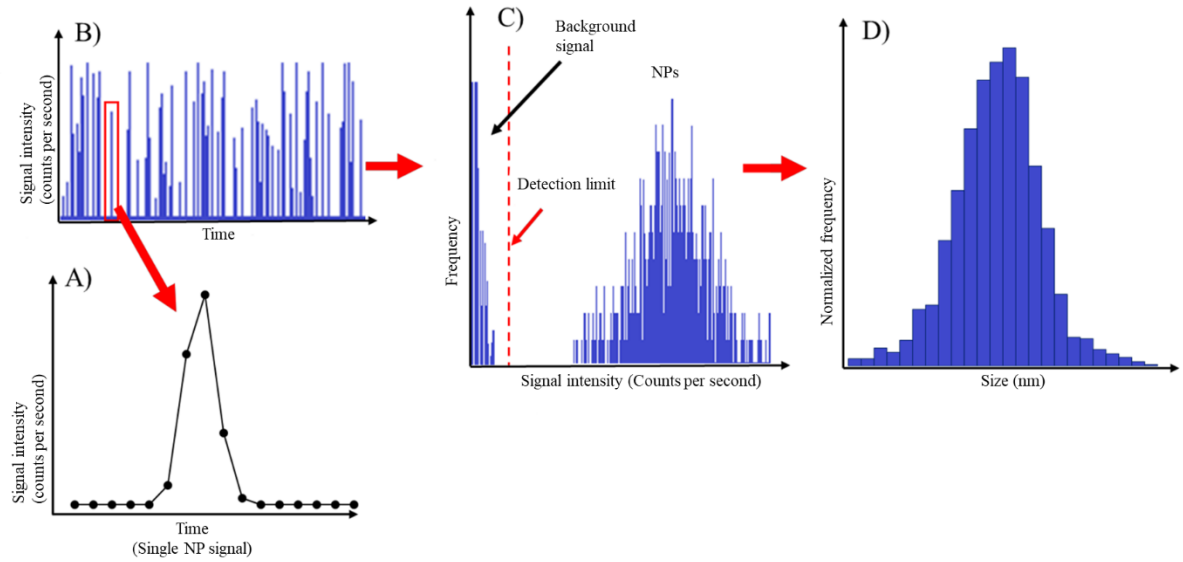

Figure 2-3: Different plots generated by the MH software during an analysis. Figure used with permission [24]

The ICP instruments rely on calibration routines to accurately calculate the mass and, subsequently, the size, of NPs. An ideal situation would be to run analysis of NP-standards with exact and certified composition, density, and shape for a direct calibration. However, few CRMs aimed at nanotechnology are available on today's method. Another method is based on the calculation of the nebulization efficiency (NE). NE describes the ratio of the amount of analyte being nebulized to the amount of analyte that reaches the plasma. There are a few different techniques to calculate the NE. In this project, a NP size-calibration method is used, where a NP reference material with known sizes is used in combination with an ionic standard of the same material. The sensitivity difference between the signal per ng analyte from the ionic solution and the signal per ng analyte from the NP suspension gives the NE. Au 60 nm NPs in combination with ionic Au standard was used to calculate NE

2.2.3 Sp-ICP-MS Equations

The following equations are used by the MassHunter software to perform the necessary ICP-MS calculations [21].

Response factor, s (cps/ppb)

$$s = \frac{I_{ion} - I_{blk}}{C_{ion}}$$ **Equation** 2.1

I_{ion}= Mean signal from ionic std. (cps)

I_{blk} = Mean signal from ionic blank (cps)

C_{ion}Concentration of ionic std.

Standard mass of particle, m_{std}, (fg) of the reference material

$$m_{std} = \frac{4}{3}\pi \times \left(\frac{d_{std}}{2 \times 10^7}\right)^3 \times p_{std} \times 10^{15}$$ **Equation** 2.2

p_{std} = Density of the reference material (g/cm^3)

d_{std} = Diameter of the reference material (nm)

Nebulization efficiency, η_n, particle size method

$$\eta_n = \frac{\frac{4}{3}\pi \times \left(\frac{d_{std}}{2}\right)^3 \times \rho_{std} \times s \times 60}{l_p \times t_d \times V \times f_d \times 10^{12}}$$ **Equation** 2.3

l_p = Top intensity of reference material (cps)

f_d= Ratio of the molar mass of the NP and the molar mass of the analyte (e.g., molar mass TiO_2/Ti)

V = Sample uptake (mL/min)

t_d = integration time (sec)

S = response factor (cps)

Mass of a single NP in the reference material, m_{p_n} (fg)

$$m_{p\_n} = \frac{I_{rn\_n}}{\overline{I_{rm}}} \times m_{std}$$ **Equation** 2.4

I_{rn} = Single signal of NP from reference material (cps)

$\overline{I_{rm}}$ = Mean particle signal from reference material (cps)

Particle number concentration of sample and reference material, C_p (particles/L)

$$C_p = N_p \times \frac{1}{\eta_n} \times \frac{1}{V} \times \frac{1}{T} \times 10^3$$ **Equation** 2.5

η_n = Nebulization efficiency

Mass of a single NP, m_{p_n} (fg)

$$m_{p\_n} = I_{p\_n} \times \frac{1}{s} \times t_d \times V \times \eta_n \times 10^3 \times f_d \times \frac{1}{60}$$ **Equation** 2.6

I_{p_n} = intensity of a single NP signal

Mass concentrations of NPs in samples and reference material, C_m (ng/L)

$$C_m = \frac{\Sigma m_p}{10^3} \times \frac{1}{\eta_n} \times \frac{1}{V} \times \frac{1}{T}$$ **Equation** 2.7

m_p = mass of a single NP (fg)

Size of a single NP in a sample and in a reference material, d_{p_n}, (nm)

$$d_{p\_n} = \sqrt[3]{\frac{6}{\pi} \times \frac{m_{p\_n}}{10^{15} \times \rho_p} \times 10^7}$$ **Equation** 2.8

ρ_p = Density of analyte (g/cm^3)

2.2.4 Scanning electron microscopy

In SEM, images are produced as a result of interactions between a beam of electrons and atoms across multiple layers in the sample, generating various signals which can be detected to give information of the surface topography [25]. **Figure** 2-4 shows the main components in a SEM instrument. A standard SEM instrument uses an electron gun to produce the electron beam, electromagnetic lenses to focus the beam on the sample, a secondary-electron detector, and a backscattered electron detector. The most common imaging mode is by collecting signals from secondary electrons, which are usually very low in energy (<50 eV). The secondary electrons are electrons ejected from electron bonds between atoms within a few nm of the sample as a result of interactions with beam electrons. Due to the low energy, high degree of localization at the point of impact with the electron beam, and small wavelengths it is possible to generate images with resolutions below 1 nm.

Backscattered electrons are higher in energy as they are reflected from the sample, thus the resolution is less than for secondary electrons. However, this method is used in analytical SEM as the intensity of backscattered electrons are related to the atomic number of the sample. SEM analysis depends on the conductivity of the sample, and non-conductive samples are usually coated with a conductive metal/metal combination such as Au, Au/Pd, Pt, Ir, W, and more, as a part of the sample preparation. In this thesis, the samples are coated by a Au/Pd alloy.

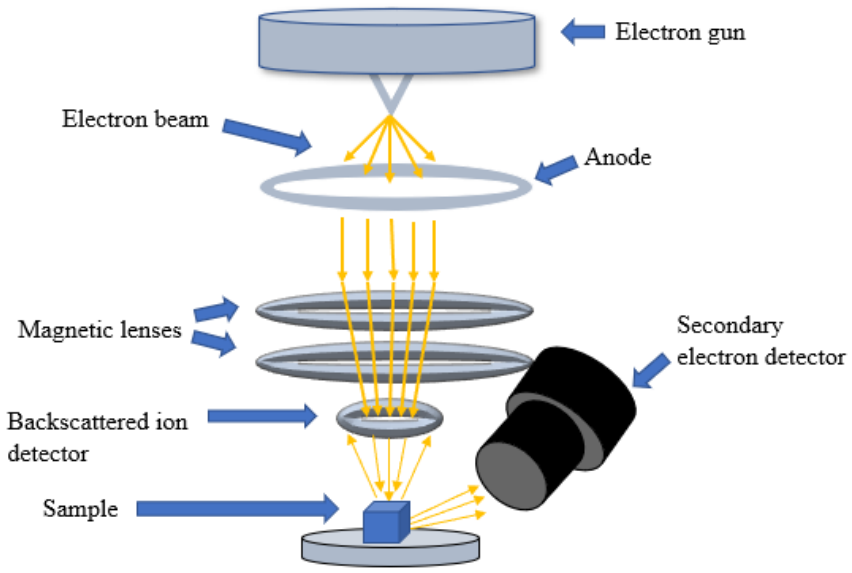

Figure 2-4: Main components in a SEM-instrument.

2.3 Mathematical Equations

Stokes Equation

$$v = \frac{d^2(p - L) \times g}{18n}$$ **Equation** 2.9

v = Velocity of particle moving through medium.

d = Diameter of particle.

p = Particle density.

L = Medium density

n = Viscosity of medium

g = Gravitational force

Relative centrifugal force, RCF

$$RCF = 11{,}18 \times r \times \left(\frac{RPM}{1000}\right)^2$$ **Equation** 2.10

r = Distance between particles and the center of rotation (cm)

Standard deviation, SD

$$SD = \sqrt{\frac{\Sigma_{i=1}^{n}(xi - \bar{x})^2}{n - 1}}$$ **Equation** 2.11

xi = Individual value from measurement

$\bar{x}$ = Average of measurements

n = number of measurements

Relative standard deviation, RSD (%)

$$RSD(\%) = \frac{SD}{\bar{x}} \times 100$$ **Equation** 2.12

SD = Standard deviation

Measurement uncertainty

$$MU = 2 \times RSD(\%)$$ **Equation** 2.13

RSD (%) = Relative standard deviation

Limit of detection, LOD

$$LOD = \bar{x} + 3 \times SD$$ **Equation** 2.14

Limit of quantification, LOQ

$$LOQ = 3 \times LOD$$ **Equation** 2.15

3. Experimental

3.1 Materials and instruments

Table 3-1: Overview of instruments and equipment used.

Instruments and equipment
Wirlmixer, IKA MS1 minishaker
SEM Zeiss Supra 55 VP
Polaron SC502 sputter coater (for SEM analysis)
Heidolph shaker incubator
Millipore Milli-Q ® water purification system 18.2 MΩ.cm
15 mL and 50 mL polypropene centrifuge tubes
13 mL roundbottom polypropene tubes
120 mL polypropene beakers for Milli-Q® water.
50 mL volumetric flask
100 mL volumetric flask
Eppendorf finnpipettes
Weighing boats
SP-S4 Autosampler for ICP-MS
Agilent 8900 ICP-MS
Eppendorf™ 5702 centrifuge
A-4-38 Swing Bucket Rotor
Bandelin™ SONOPULS HD 2070 probe sonicator
SPEX SamplePrep Freezer/Mill 6875D cryomill

Table 3-2: Overview of chemicals used

Chemical	**Manufacturer**	**Product number**
Au NPs 60 nm 50 mg/L citrate stabilized	NanoComposix	AUCN60
Ceo2 30-50 nm 20% w/w 2.5% acetic acid	Sigma-Aldrich	289744
Au ionic std. 1001 ± 6 µg/mL in 2% HNO_3	Spectrascan	SS-1118N
HNO_3 3.5%*	-	-
Ce ionic std. 1000 mg/L ± 2 mg/L in 5% HNO_3	Sigma-Aldrich	16734
Protease from Bacillus sp.	Sigma-Aldrich	P0029
Tuning solution for ICP-MS 1 µg/L Ce, Co, Li, Mg, Ti og Y in 2% HNO_3	Agilent	5185-5959
TiO2 < 150 nm NPs, mixture of rutile and anatase, 33 - 37 wt. % in water	Sigma- Aldrich	700347
Ti ionic std. 1000 mg/L ± 2 mg/L in 2% HNO_3	Sigma- Aldrich	12237

3.2 Preparation of biological samples

Due to the lack of CRM-matrices for nanoanalytical purposes, biological samples were used to investigate the content, stabilization, and extraction of spiked and natural NPs. The biological samples that are used in this thesis are mussels (*Mytilus edulis*) and Atlantic cod (*Gadus morhua*). The samples were handled and prepared by staff at IMR according to the respective in-house routine for sample pretreatment.

The mussels analyzed in this project stems from a surveillance project at IMR focused on the concern for a declining population in Norway. The frozen mussels were thawed over 24 hours in a sealed bag of lukewarm water before properly washing and scrubbing in running water to remove beard, sand, and debris. The shells were opened by cutting the adductor muscles with a butter knife. Any excess impurities such as grime and sand were flushed away using distilled water. The mussels were left to dry off on paper towels for 5 minutes before the entire entrails of the mussels were scraped out and transferred to a mesh strainer for further runoff. The entrails were then homogenized over two rounds. Firstly, in a standard kitchen blender (Phillips HR1371), and subsequently in a homogenizer (POLYTRON System PT 2100). Finally, the homogenate was packed and frozen in plastic boxes. Originally, the mussels were harvested from different locations along the Norwegian coast to identify geographical variation in bacterial content, deceases and more. For this thesis, the geographical element was not considered.

In contrary to the mussels, the cod samples specifically consist of only the side fillet of the fish. The purpose of this was to keep the natural background of TiO_2 as low as possible. Whereas mussels are filter feeders and inhabit areas generally more exposed to NPs [26], fish fillet will not have the same uptake due to lack of access combined with limited potential uptake in a muscle. The preparation starts by making an incision from the anus to the head and remove the intestines. The dissection is done while the fish is still not completely thawed as fat cells are destroyed upon freezing and will easily flow out and cause contamination when thawed. The process proceeded by cutting over the esophagus without puncturing the gallbladder and making a cut from the neck along the spine. The fillet was then removed by letting the knife slide along the spine until the fillet was detached. Visible bones and skin were removed with tweezers and knife, respectively. The fillet was cut into cubes before homogenized in a standard kitchen blender (Phillips HR1371). While the sample preparation process for muxssels seemed to be successful, creating a smooth homogenous mass, the results for cod fillet were less optimal for enzymatic digestion as the mass contained visible muscle fibers and had an overall

grainier consistency. Further measures were made by milling the processed cod fillet in a cryomill (SPEX SamplePrep Freezer/Mill 6875D). The standard machine protocol for meat (including fish) were used to obtain the final homogenate.

3.3 Enzymatic digestion

The biological matrices were enzymatically digested by using proteolytic enzymes, also called protease, from the bacterium *Bacillius sp.* The product is marketed under the name Protamex®. In the bacteria, the main function of protease is to catalyze the introduction of water (hydrolysis) on peptide bonds in proteins causing the protein to be broken down to its constituent amino acids[27]. This method of enzymatic digestion is validated at IMR for extraction of Au NPs from mussels [5]. For the digestion process, a 20% (w/v) solution of Protamex® was made by weighing 10 g of Protamex® into a 50 mL volumetric flask and filling it up to the mark with Milli-Q® water. In order to sufficiently dissolve the enzyme powder, the flask was filled with approximately 25-30 mL Milli-Q® water and shaken before filling it up to the mark. Protamex® was added to mussel samples, both spiked and unspiked, and blank samples, also spiked and unspiked (**Figure** 3-1). This was done parallel to instrument blanks to give an understanding of the contribution and effect of Protamex® on the recoveries of NPs. 1 g of wet sample or 1 mL of Milli-Q® water is added to a 13 mL round bottom test tube, depending on whether it was a matrix sample or blank without matrix. The spike-samples were spiked with 100 µL of a NP dispersion with known concentration. The concentration varied depending on which particles that were analyzed. The validated concentration for the Au NP spike solution was 500 µg/L. More details for CeO_2 and TiO_2 spiking concentration later in this chapter. All the test tubes were shaken for 15 seconds before adding 3.0 mL of 20% Protamex® solution, minus the amount of spiked solution. E.g., 2.8 mL of enzyme solution was added if the sample is spiked with two different NP dispersions. For the method blanks, the same volume of Milli-Q® water is added accordingly. The samples are vortexed again for 15 seconds before placing the entire rack of samples in a shaking incubator for 1 hour at 50 °C and 300 RPM. After this, 4 mL of Milli-Q® water was added to the test tubes and vortexed at full speed for 15 seconds before immediately diluting 2 mL from each sample to 10 mL. The samples were then vortexed for another 15 seconds at full speed before 1 mL from each sample was diluted to 12.5 mL, this time in 15 mL centrifuge tubes. By this approach, all samples were diluted in total 500 times and the theoretical concentration of spiked Au NPs should be 100

ng/L. The samples were then vortexed again for 15 seconds at full speed, and analyzed by sp-ICP-MS. All dilutions in Milli-Q® water.

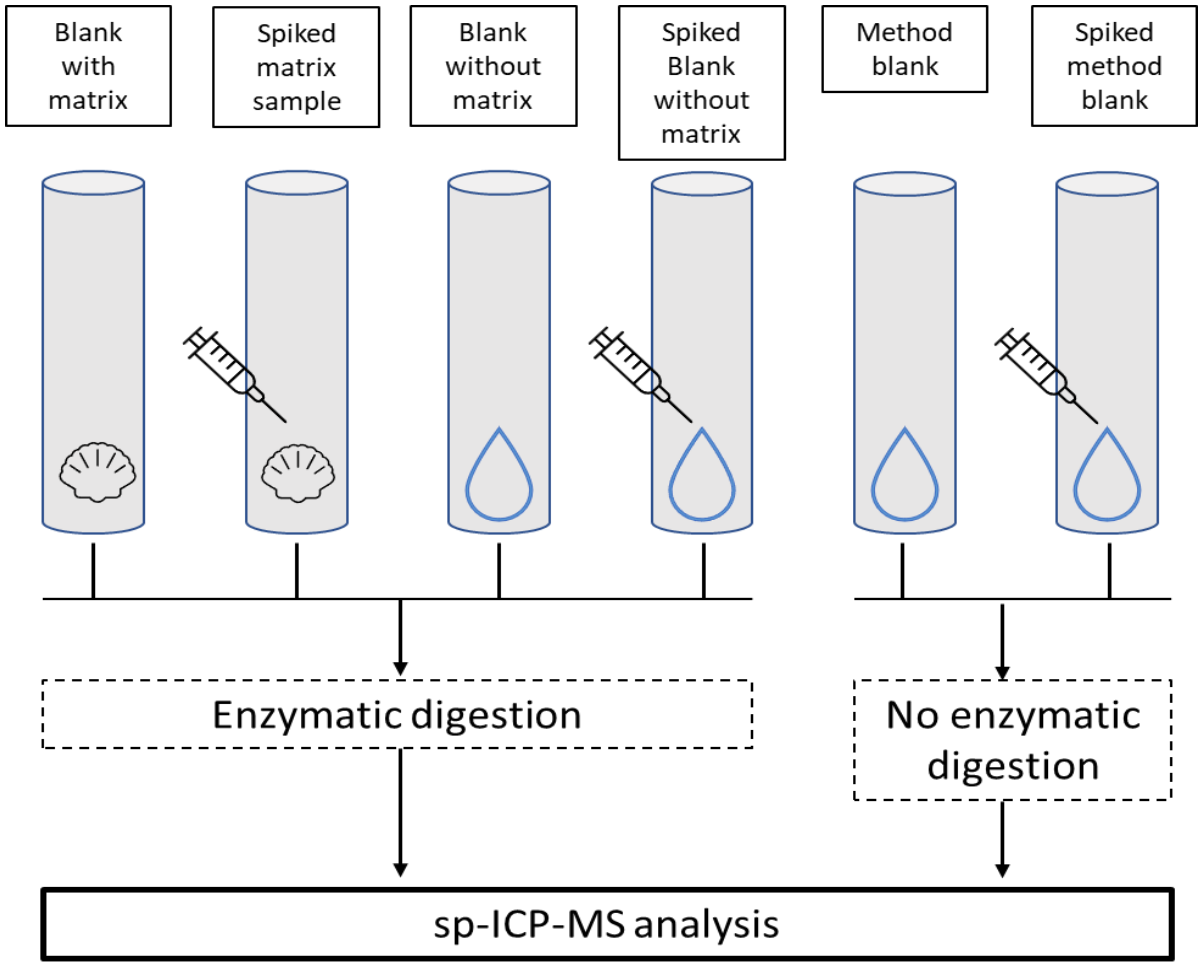

Figure 3-1: Different types of sampling and spiking used in recovery analysis.

An adjustment to this method was made when working with TiO_2 NP recovery analysis in cod fillet. For this procedure, a 2% Protamex® solution was used instead of the 20% solution previously used. The 2% solution was made by weighing in 1 g of Protamex® and dissolving it in a 50 mL volumetric flask. The samples were incubated at 50 °C overnight for 18 hours as this adaptation of the validated method was expected to require longer time in the incubator to achieve complete digestion of tissue due to the significantly lower amount of enzymes present. The incubated samples were diluted 500 times in the same way as the validated method, before analyzing by sp-ICP-MS.

3.4 Refinement process of CeO_2 NPs and TiO_2 NPs

The NPs used in the refinement process stems from the same stock solutions as the unrefined NPs. It is worth noting that the word "refining" should in this context be understood as a filtering procedure based on the size of the NPs and not as an attempt to change the size or properties of any individual NPs. The speed and time of the centrifugating is decided and calculated based on the stokes Equation (**Equation** 2.9**)**. The calculations were assisted by an online tool [28] which was originally designed for calculation of centrifugal pelletizing of vesicles in biological samples. The calculator uses input values from the rotor type, diameter, and length between rotor center and the medium as well as medium viscosity and density, and the density of the vesicles, which is attributed to the density of the NPs in this project. The cutoff value is set at 70 nm and 100 nm for CeO_2 and TiO_2 NPs, respectively, meaning that all NPs above the cutoff size should theoretically be pelletized. The centrifuge used is an Eppendorf™ 5702 with an A-4-38 Swing Bucket Rotor. Some samples are probe sonicated using a Bandelin™ SONOPULS HD 2070 Homogeniser. All dilution and use of water is done with Milli-Q® water.

3.4.1 Refinement of CeO_2 NPs

A 10 mg/L suspension of CeO_2 30-50 nm NPs was prepared by diluting 250 µl of stock suspension (20% $^{w}/_{w}$) to 10 mL in a 15 mL centrifuge tube (5000 mg/L). From this, 2.5 mL was diluted to 50 mL in two separate 50 mL centrifuge tubes, T1 and T2. Only T1 will be subjected to probe sonication for comparison possibilities. Both tubes were shaken by hand before they were stirred in a vortex shaker for 15 seconds. The two 50 mL tubes were centrifuged for 14 minutes at 4400 rpm which theoretically gives a cutoff at 70 nm. When completed, the upper 48 ml of each tube was carefully removed by constantly pipetting out the top layer (pipetted out 9 x 5 mL + 1 x 3 mL). The removed water was then replaced with new water (48 mL). The tubes were again shaken by hand and vortexed until the NPs, including the sedimented precipitate, appeared to be completely dispersed. T1 were then probe sonicated for 30 seconds at 60% power with 0.9 seconds active intervals and 0.1 seconds passive interval (pulsed cycle 9) before both T1 and T2 were centrifuged again. This cycle was repeated 4 more times until T1 was centrifuged and probe sonicated five times and T2 was centrifuged 5 times. The final product was then diluted 100 times before analyzed by sp-ICP-MS. An aliquot of 100 µL was taken out and diluted into 10 mL from each tube before every centrifugation. The

aliquots from step 1-5 were then further diluted until optimal concentrations were found by sp-ICP-MS analysis.

3.4.2 Refinement of TiO_2 NPs

A 70 mg/L suspension of TiO_2 <150 nm NPs were prepared by diluting 100 µL of stock suspension (33-37% $^{w}/_{w}$) to 10 mL in a 15 mL centrifuge tube (3500 mg/L). From this, 1 mL was further diluted to 50 mL in a 50 mL centrifuge tube (70 mg/L). The suspension was shaken by hand and vortexed for 15 seconds before centrifuged for 35 minutes at 4400 RPM which theoretically gives a cutoff at 100 nm. This created a pellet of agglomerated NPs in the bottom of the centrifuge tube. The medium, containing the dispersed NPs not agglomerated in the bottom, was immediately decanted out and disposed, leaving only the NP-pellet in the centrifuge tube. The disposed medium was replaced by 50 mL of Milli-Q® water. As the pellet would not disperse by shaking either by hand or vortex stirring, the tube was probe sonicated for 30 seconds at 70% power with 0.9 seconds active intervals and 0.1 seconds passive intervals (cycle 9) to completely disperse the pellet. The centrifuge tube was then centrifuged again, and the refinement process is complete when the sample is centrifuged, and probe sonicated in total five times. An aliquot of 100 µL was taken out and diluted into 10 mL from each tube before every centrifugation. The aliquots from step 1-5 were then further diluted until optimal concentrations were found by sp-ICP-MS analysis.

An extra step was added to examine the possibility to further manipulate the size distribution by decreasing the number of larger particles in the suspension. This was done by centrifuging an aliquot of 10 mL from the refined suspension in a 15 mL centrifuge tube for five minutes at 4400 RPM and finally pipetting out and disposing the top 9 mL in the same way as for CeO_2 refinement. The remaining 1 mL was diluted to 10 mL and probe sonicated for 15 seconds at 50% power at with 0.5 active interval and 0.5 second passive interval and finally analyzed by sp-ICP-MS.

3.5 sp-ICP-MS analysis

All sp-ICP-MS analysis included in this project were performed on a 8900 Triple Quadrupole ICP-MS instrument from Agilent Technologies. The instrument was tuned before every sequence with a ICP-MS tuning solution from Agilent containing 1 µg/L each of Li, Mg, Y, Ce, Ti and Co in a matrix of 2% HNO_3. All samples were measured for 120 seconds. However, many sequences were performed in multi-element mode. In multi-element mode, different analytes in the same sample are measured with respect to the relevant *m/z* values, which drastically increases the sample time, as the instrument does not measure "all at once" but switches the *m/z* after one is finished. The analysis of CeO_2 NPs and Au NPs was done using a single quadrupole with no additional mass filtering. For analysis of TiO_2 NPs the triple quadrupole technology was utilized as the most abundant isotope ^{48}TI (73.7%) on mass-shift mode with O_2 + H_2 as collision gas. In all analytic sequences a 60 nm Au NP reference material and a 10 µg/L ionic Au reference solution was used in combination with an ionic blank solution to linearly calibrate the instrument. The ionic blank solution consisted solely of Milli-Q® water. In addition to this, a 1 µg/L ionic Au solution was analyzed as a control sample to check linearity. A 10 µg/L ionic reference solution of the analyte metal of interest was also measured. For instance, if TiO_2 NPs were to be analyzed, a 10 µg/L of ionic Ti were measured as an analytic reference. Between each sample measurement, the machine was rinsed with 5% HNO_3 for 60 seconds and Milli-Q® water for 90 seconds. To the best of our ability, the sequence order was conducted from highest to lowest in analyte concentration to minimize carry-over and contamination of the instrument. Control sample of Milli-Q® water was measured in between approximately every third sample, or more often, when necessary, to monitor the amount of carry-over and for the sake of flushing the tubing system. The dwell was set at 100 µs which results in 1.2 million data points generated per sample.

3.5.1 Dilution and analysis of Au 60 nm NPs.

Au 60 nm NPs were analyzed at *m/zi* 197 with a concentration of 100 ng/L as a reference material for the determination of NE. In addition to this, Au NPs were analyzed as an analyte in multielement (cod) and single element (mussels) mode for recovery tests in mussels and cod filet. In this case, the matrix was spiked with 100 µL of 500 µg/L in order to obtain a concentration of 100 ng/L after the final dilution of the digested samples.

3.5.2 Dilution and analysis of refined and unrefined cerium dioxide 30-50 nm NPs

Unrefined CeO_2 30-50 nm NPs were analyzed at concentrations 100 ng/L and 200 ng/L in multi and single element mode. The concentrations were prepared by stepwise dilution in Milli-Q® water of a 20% ($^{w}/_{w}$) stock NP-suspension containing 2.5% acetic acid. From stock suspension, 2.5 mL was diluted to 10 mL (50 000 mg/L). From this, 1 mL was diluted to 10 mL (5000 mg/L), and from this, 100 µL was diluted to 10 mL (50 mg/L). A 500 µg/L suspension was made by diluting 100 µL of 50 mg/L suspension to 10 mL, and from this a 5 µg/L was made by diluting 100 µL to 10 mL. Finally, the 100 and 200 ng/L were prepared by diluting 200 and 400 µL, respectively, of 5 µg/L suspension to 10 mL. All steps include 10 seconds of vortex stirring. The 500 µg/L was used to spike mussel samples to obtain an end concentration of 100 ng/L after the enzymatic digestion procedure according to the validated method for Au NPs in mussels (chapter 3.3).

For the refined suspension, the starting concentration is unknown as it is impossible to precisely calculate the concentration of a suspension after a centrifuge cycle in the refinement process (chapter 3.4), nor is the concentration very significant in this case. Due to this uncertainty, a NP number based approach was used for refined NPs. For the analysis, refined CeO_2 NPs were found to obtain optimal concentration for sp-ICP-MS analysis when diluted by a factor of two million in a 4-step process in Milli-Q® water. Firstly, 100 µL of the refined stem suspension was diluted to 10 mL (diluted 100x). A spike suspension was prepared by further diluting 2.5 mL of this suspension to 7.5 mL (diluted 400 x). from this, 100 µL was diluted to 10 mL (diluted 40 000x) and lastly, 200 µL of this was diluted to 10 mL (diluted 2 000 000x). All CeO_2 NPs were analyzed with *m/z* at 140.**Table** 3-3 shows the instrument parameters used in the analysis of CeO_2 NPs.

Table 3-3: Instrument parameters (Agilent 8900 and SPS4 autosampler) for the analysis of CeO_2 NPs.

Sp-ICP-MS parameter	**Value**
Mode	Single quadrupole
RF power	1550 W
Nebulizing gas	1.05 L/min
Nebulizer	MicroMist
Pneumatic pump	0.1 rps
Integration time	100 µs
Monitored isotope	140 Ce
Analysis time per sample	120 s
Tube ID	1.02 mm

3.5.3 Dilution and analysis of refined and unrefined Titanium dioxide <150 nm NPs

Unrefined TiO_2 NPs were for the recovery test in cod analyzed with a concentration at 70 ng/L by diluting the stock suspension (~ 35% $^{w}/_{w}$) by a factor of five billion in Milli-Q® water. This was done by diluting 100 µL of stock suspension to 10 mL. A spike suspension was made by further diluting 100 µL two more times to 10 mL. Finally, the 70 ng/L analyze-suspension was made by diluting the spike suspension by a factor of five thousand in a twostep process where firstly 100 µL, and then 200 µL were diluted to 10 mL, respectively. Due to the longer incubation time for TiO_2 NPs in cod matrix, the 70 ng/L suspension in Milli-Q ® water was analyzed the same day, while the incubated samples were analyzed the next day. The

As for the refined CeO_2, the concentration of refined TiO_2 NPs is difficult to presume with any precision, so a number based approach was used in this case as well. For the analysis, refined TiO_2 NPs were found to obtain optimal concentration for sp-ICP-MS analysis when diluted by a factor of 150 000 in a 3-step process with Milli-Q® water. A spike dispersion was made by diluting 300 µL to 9 mL (diluted 30x). 100 µL of this dispersion was subsequently diluted to 10 mL (diluted 3000x), and the final analyze solution was made by diluting 200 µL to 10 mL (diluted 150 000x in total). Like the unrefined TiO_2 NPs, refined TiO_2 NPs in Milli-Q® water were analyzed the same day, and the incubated samples were analyzed the next day, due to the prolonged incubation time

Table 3-4: Instrument parameters (Agilent 8900 and SPS4 autosampler) for the analysis of TiO_2 NPs.

Sp-ICP-MS parameter	**Value**
Mode	Tandem (MS/MS)
Monitored mass Q1	48 amu
Monitored mass Q2	64 amu
Reaction gas	$H_2 + O_2$
RF power	1550 W
Nebulizing gas	1.05 L/min
Nebulizer	MicroMist
Pneumatic pump	0.1 rps
Integration time	100 µs
Analysis time per sample	120 s
Tube ID	1.02 mm

3.5.4 Dilution of ionic standards

The ionic standards for the reference material and analytes were diluted from 1000 mg/L stock solutions to 1 µg/L and 10 µg/L through a three-step dilution process. The dilution of ionic Au reference standard was diluted using only Milli-Q® water. For ionic Ti and Ce, the solutions were diluted half and half of 5% HNO_3 and Milli-Q® water. This is because earlier tests by staff at IMR showed that diluting in 2.5% HNO_3 gave better results when analyzing Ti with sp-ICP-MS. This is most lightly due to formation of small NPs in the ionic solution as the pH increases.

From 1000 mg/L stock solution, 100 µL was diluted to 10 mL in a 15 mL centrifuge tube (10 mg/L) from here, 100 µL was diluted to 10 mL (100 µg/L). finally, the 10 µg/L standard was made by diluting 1 mL of the 100 µg/L solution to 10 mL. The linearity was controlled by combining the 10 µg/L standard solution and a 1 µg/L sample solution which was made by diluting 100 µL of the 100 µg/L solution to 10 mL.

3.6 Processing of data from sp-ICP-MS analysis.

The raw data from the sp-ICP-MS analysis was mainly processed in the MassHunter (MH) software version 5.1 (Agilent Technologies). Some analysis was processed in Microsoft Excel (Office 16, Windows 10) by utilizing a premade script that comes with the MH installation package, allowing for customized size distributions for any NP sample by bin size selection.

In the processing of raw data, the MH software allows for both upper and lower PDT. Only a lower PDT was used in this thesis.

3.7 Scanning electron microscopy

The SEM analysis and sample preparation was done at UoB`s facilities in Bergen and the Zeiss Supra 55 VP instrument was used with a voltage of 5 KV. Some of the preparation and analysis was assisted by Irene Heggstad (ELMIlab, UoB). The diluting of NPs was done at IMR on beforehand. Approximately 30 mg/L NP suspensions of Au 60 nm, unrefined CeO_2 30-50 nm, refined CeO_2 NPs, TiO_2 <150 nm, and refined TiO_2 NPs were analyzed. One drop of each suspension was pipetted on to a frosted end glass microscope slide and left to dry for 2 hours or until the suspension liquid was completely evaporated. The dried samples were coated with Au/Pd using a Polaron SC502 sputter coater. When the image quality allowed it, some of the SEM images were in addition analyzed using a software called ImageJ. ImageJ can calibrate the size scale bare given in the SEM images, allowing for individual NPs to be measured manually.

4. Results

4.1 sp-ICP-MS

4.1.1 Au 60 nm nanoparticles

Table 4-1 shows results from analysis of Au 60 nm in Milli-Q® water as a reference material for the determination of NE and of the results from the extracting of refined CeO_2 and TiO_2 NPs in mussel matrix and cod matrix, respectively. The extraction-recovery test of Au NPs in matrix with enzymes was performed as a controlling measure by comparing the results with expected values from the validation report previously produced by IMR staff. [5]. In the validation project, 60 nm Au NPs from Perkin Elmer (PE) were used, while 60 nm Au NPs from NanoComposix are used in this project. The PDT was set as a lower detection limit in both cases. The calculation of recoveries is not adjusted for contribution from naturally occurring NPs.

Table 4-1: Mean values, theoretical values, RSD (%) and recoveries (%) of particle numbers, particle concentrations, mass concentrations, FullQuant concentrations and sizes of Au 60 nm NPs spiked in mussel and cod matrix after enzymatic digestion. Theoretical value represents 100 ng/L Au NPs in Milli-Q® water. The Table also includes results from the validation report.

	N	Parameter	Particle number	Particle conc, (par/L)	Mass conc. (ng/L)	FullQuant conc. (ng/L)	Mean size (nm)	Median size (nm)
Au 60 nm NPs, 100 ng/L spiked in mussel matrix[1]	2	Mean	569	1.65×10^7	41	48	60	57
		Theoretical value	1012	3.00×10^7	66	69	59	59
		Recovery (%)	56	55	62	69	101	97
Au 60 nm NPs, 100 ng/L spiked in cod matrix[2]	4	Mean	1041	2.93×10^7	57	70	56	57
		RSD (%)	4.3	5.2	7.5	7.0	1.0	1.0
		Theoretical value	1654	4.7×10^7	102	105	59	59
		Recovery (%)	63	62	56	66	95	96
PE Au 60 nm 100 ng/L spiked in mussels, from validation report [5]	10	Mean	825	2.2×10^7	35	52	53	53
		RSD (%)	8.9	6.2	8.5	23	0.8	0.9
		Theoretical value	813	2.1×10^7	46	51	59	59
		Recovery (%)	102	102	77	104	90	91

[1] Test ran after recovery testing of CeO_2 NPs in mussel matrix in single element mode.

[2] Test ran parallel to recovery testing of TiO_2 NPs in cod matrix in multielement mode

Figure 4-1 displays values from **Table** 4-1 for particle number, mass concentration and mean size recoveries. On evaluation of the particle number recoveries, the validation report stands out with 102% against 56% and 63% for mussel matrix and cod matrix, respectively. The mass concentration recovery is also higher for the validation report with 77% against 62% and 56%

for mussel matrix and cod matrix, respectively. NanoComposix NPs spiked in mussels shows a recovery of the mean diameter of 101%, significantly higher than the PE Au NPs from the validation report at 90%.

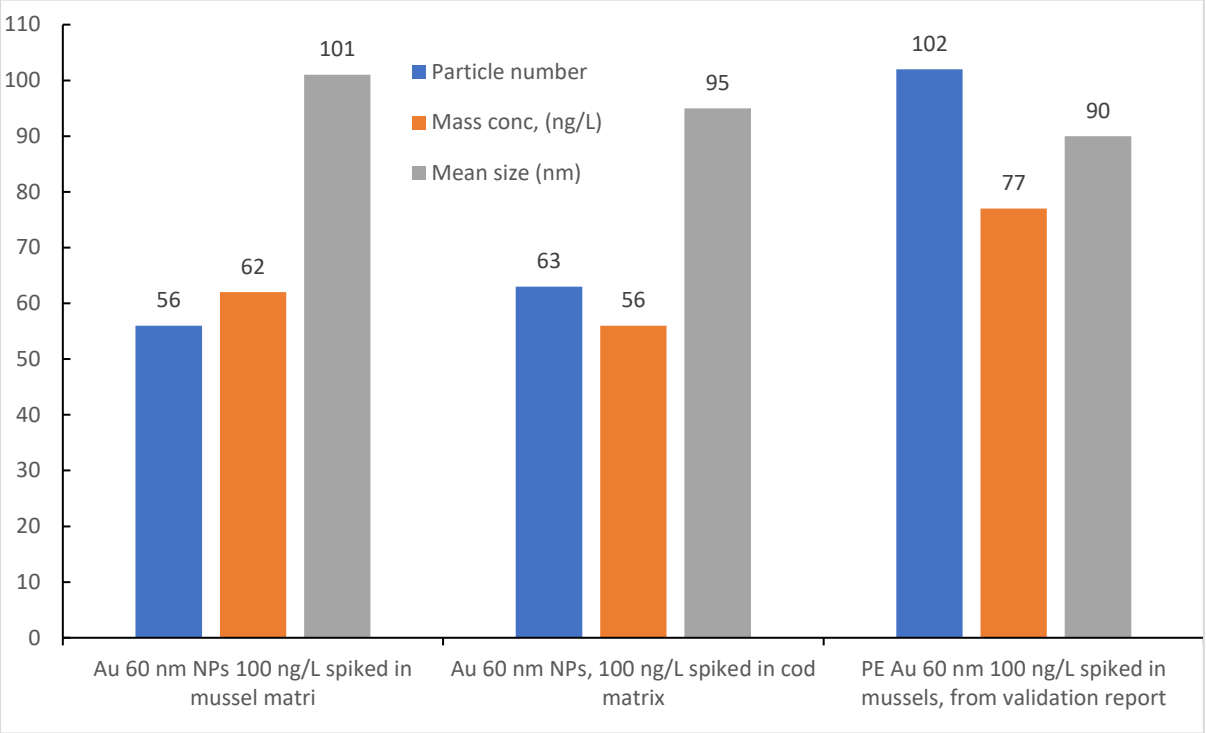

Figure 4-1: Particle numbers, mass concentrations, and Mean sizes of Au NPs spiked in cod and mussels. Includes validation results from earlier tests at IMR of spiked Au NPs in mussel matrix.

Figure 4-2 shows the normalized frequency distribution (%) of particle sizes for 60 nm 100 ng/L Au NPs in mussel matrix, cod matrix and Milli-Q® water. The NPs in Milli-Q® water (orange) obtains the most monodisperse and evenly distributed size distributing as well as the larges value for most frequently occurring size. Au NPs extracted from cod matrix (dark blue) obtains a similar distributing only shifted slightly towards a smaller size distribution. The NPs extracted from mussel matrix (light blue) obtains the lowest value for the most frequent NP diameter occurring, but still shows the largest mean value. The Figure indicates an increase in particles >65 nm compared to the two other samples.

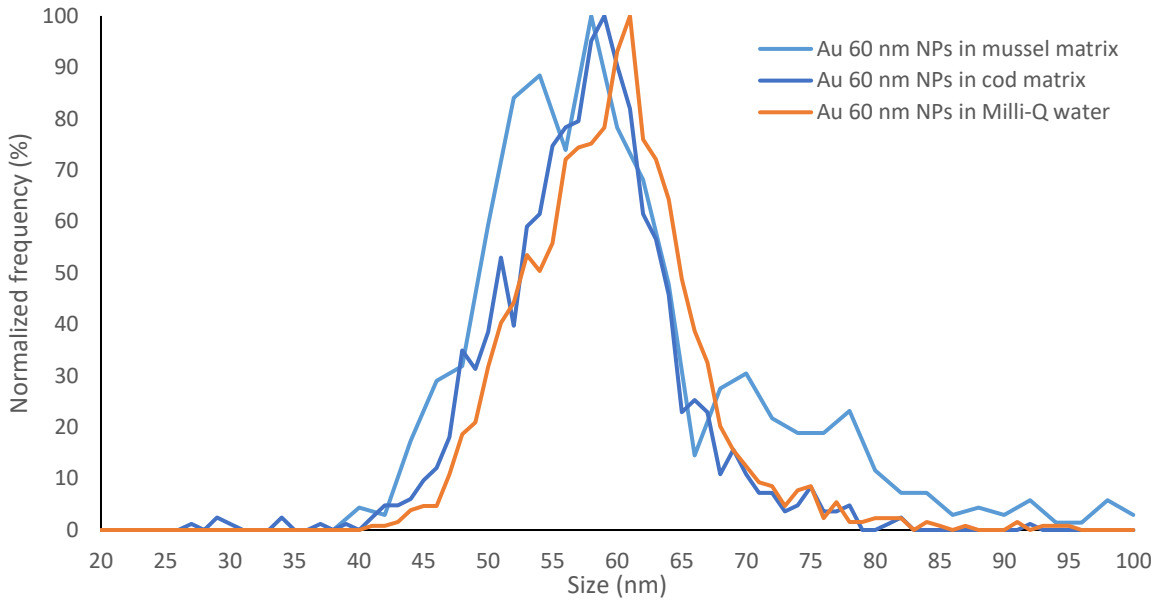

Figure 4-2: Normalized frequency (%) of particle sizes for 60 nm 100 ng/L Au NPs in mussel matrix, cod matrix and Milli-Q® water.

4.1.2 Cerium dioxide 30-50 nm nanoparticles

Table 4-2 shows the particle numbers, concentrations, and mean and median sizes for analysis of unrefined CeO_2 NPs 100 and 200 ng/L in Milli-Q® water. The mass concentrations when diluting to 100 and 200 ng/L were measured to 62 and 111, respectively. The particle numbers were given to be 2948 and 5206, respectively. The RSDs were significantly lower for the 100 ng/L suspension with values spreading from 1.7% to 9.9%. The RSDs for the 200 ng/L suspension are spreading from 11.6% to 22%.

Table 4-2: Mean values and RSDs (%) of particle numbers, particle concentrations, mass concentrations, FullQuant concentrations and sizes of unrefined 100 and 200 ng/L CeO_2 NPs in Milli-Q® water.

Sample	N	Parameter	Particle number	Particle concentration (part/L)	Mass concentration (ng/L)	FullQuant concentration (ng/L)	Mean size (nm)	Median size (nm)
CeO_2 30-50 nm 100 ng/L	3	Average	2948	7.0×10^8	62	54	49	41
		Min-max	2896-2994	6.2-7.4 ($x10^7$)	56-66	49-57	48-50	39-42
		RSD (%)	1.7	9.9	8.5	7.8	2.3	4.2
CeO_2 30-50 nm 200 ng/L	3	Average	5206	1.2×10^8	111	96	51	42
		Min-max	4513-5589	1.1-1.4 ($x10^8$)	90-137	77-119	49-52	41-43
		RSD (%)	11.6	12.3	21.3	22.0	3.0	2.7

4.1.3 Refined cerium dioxide nanoparticles

Table 4-3 shows the results from the analysis of a suspension from each step in the refinement process of CeO_2 30-50 nm NPs, including before the process started (times centrifuged = 0). The values in the Table stems from the analysis of the T2 parallel which did not include probe-sonication. A steady increase in the size-parameters is observed, from 42 nm to 84 nm in mean size, except for the second to last step. As mentioned in chapter 3.5.2, the dilution of the suspensions was done with respect to the particle number as this is a tangible approach to quickly assess further dilution. A particle number between 1000 – 4000 was assessed to be optimal. As a result of increasing sizes while particle number is kept above 2-3000, the mass concentration is also increasing drastically. After 4 repetitions of the refinement cycle, the suspension was not optimally diluted, giving a particle number of 7529, which also gives the impression of larger sizes for this step than the next.

Table 4-3: Stepwise overview of the refinement process for CeO_2 30-50 NPs. Values in the Table are from the non-sonication version of the refinement process (T2)

Times centrifuged	Particle number	Mass conc. (ng/L)	FullQuant conc. (ppb)	Mean size (nm)	Median size (nm)	Most frequent size
0	2692	64.0	0.055	51	42	28
1	1864	75.0	0.062	67	62	56
2	3096	243.7	0.199	83	76	66
3	4358	359.5	0.294	87	82	74
4	7529	724.3	0.590	94	90	82
5	3152	262.4	0.214	89	84	74

Figure 4-3 shows the stepwise overview of the particle size distributing during the refinement process for CeO_2 30-50 nm NPs. The top left gives the size distribution of the untreated stock dispersion, which shows that the majority of the NPs are in the lower region of the detectible size range, from 25-40 nm.

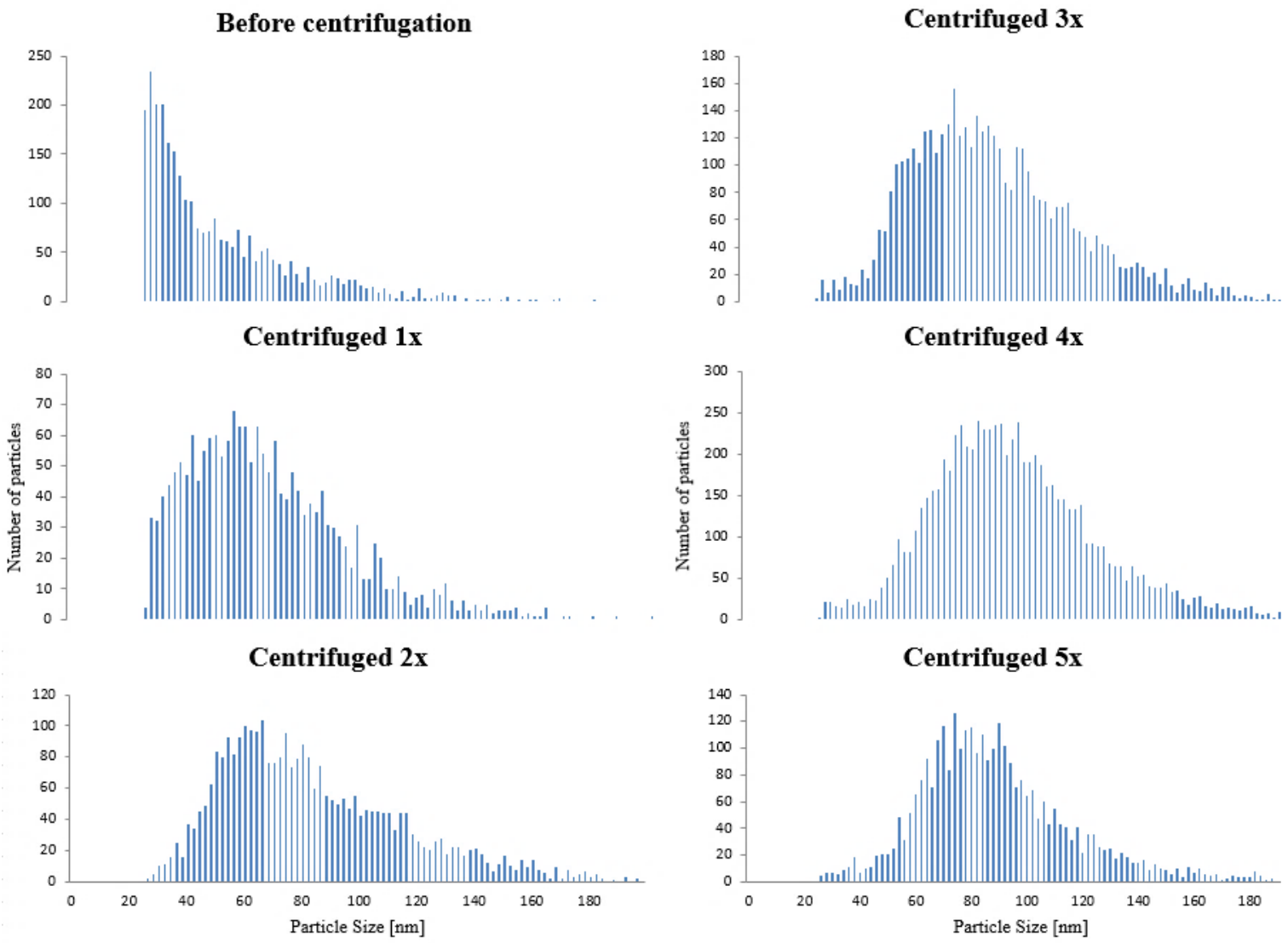

Figure 4-3: The stepwise overview of the particle size distribution during the refinement process for CeO_2 30-50 nm NPs.

The perhaps largest change comes after the first cycle in the refinement process where a clear shift towards larger particles sizes is observed in the Figure. Steps 2, 3, and 4 shows a gradually increasing size of the distributing when observing the tops of the distributions – the most frequent occurring sizes. When the refinement process is finished after five cycles, the distributing obtains a relatively evenly distributed, more monodisperse, gaussian-like shape which is easily accounted for by sp-ICP-MS.

Table 4-4 and **Figure** 4-4 compares the mean, median, and most frequent sizes of the NPs from the analysis of the refined products T1 and T2, where T1 was probe sonicated every cycle in addition to the centrifuging. The results do not differ significantly, although the RSDs of the sonicated NPs is noticeably higher. In the mean and most frequent sizes the RSDs of T1 are

6.1% and 10.9%, respectively, against 3.7% and 7.0% for T2. This is reflected in the min-max values in **Table** 4-4 which shows a larger size and particle number span for T1 than T2.

Table 4-4: Comparison between the T1 (centrifuged and probe-sonicated) and T2 (centrifuged only) versions of the refinement process for CeO_2 30-50 nm NPs.

Sample type	N	Parameter	Particle number	Mean size (nm)	Median size (nm)	Most frequent size (nm)
CeO_2 NPs, Centrifuged and sonicated	4	Mean	3431	100	94	83,5
		Min-max	2679-4071	91-104	85-99	74-94
		RSD (%)	19,8	6,1	6,8	10,9
CeO_2 NPs, Centrifuged only	4	Mean	2803	101	98	95
		Min-max	2305-3364	99-104	93-101	86-102
		RSD (%)	15,7	3,7	4,04	7.0

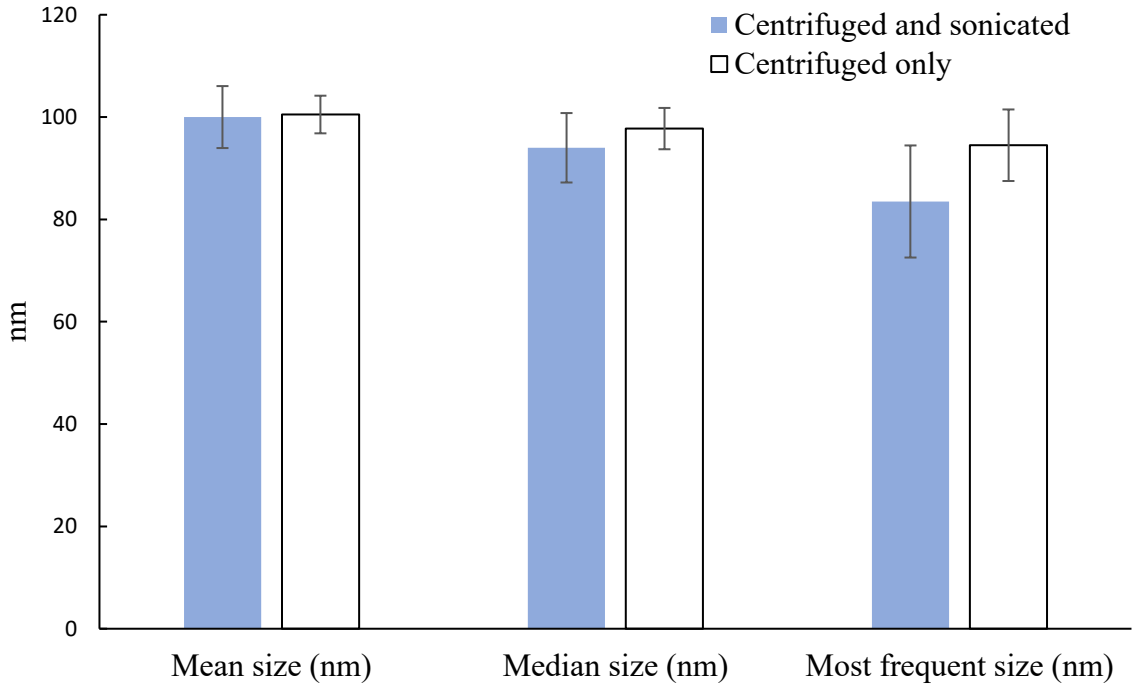

Figure 4-4: Comparison between the T1 (centrifuged and probe-sonicated) and T2 (centrifuged only) versions of the refinement process for CeO_2 30-50 nm NPs. Error bars shows RSD.

Table 4-5 shows the results from the extraction- recovery analysis of refined CeO_2 NPs spiked in mussel matrix. When adjusted for the natural contribution, the recoveries for particle number and mass concentration were found to be 78% and 83%, respectively. The mean diameter of the natural CeO_2 NPs extracted from the unspiked mussel samples were measured to 61.5 nm, well separated from the mean diameter of CeO_2 NPs extracted from spiked samples at 94 nm.

Table 4-5: Mean values, RSDs and recoveries of particle numbers, particle concentrations, mass concentrations, FullQuant concentrations and sizes of refined CeO_2 NPs spiked in mussel matrix with enzymatic digestion and in Milli-Q® water.

Samples	N	Parameter	Particle number	Particle conc. (par/L)	Mass conc. (ng/L)	FullQuant conc (ng/L)	Mean size (nm)	Median size (nm)
Refined CeO_2 NPs in MilliQ	2	Mean	3418	9.20×10^7	427	349	99	97
		Min-max	3386-3450	9.10-9.30 (x 10^7)	419.2-434.8	343-355	99-99	96-97
Natural CeO_2 NP in mussel samples	2	Mean	559	1.50×10^7	26	135	61.5	51
		Min-max	551-568	1.5-1.5(x10^7)	23.9-29.2 x 10^7	133-138	61-62	49-52
CeO_2 in spiked mussel samples	4	Mean	3217	8.65×10^7	380.78	432	94	93
		Min-max	3166-3315	8.5-8.9 (x 10^7)	362-392	417-445	94-95	92-93
		RSD (%)	2.2	2.2	3.8	3.2	0.5	0.5
		Recovery (%)	78	78	83	85	95	96

Figure 4-5 shows the normalized size frequencies of the refined CeO_2 NPs in Milli-Q® water (blue) and the same particles spiked and extracted from mussels after enzymatic digestion (orange). **Table** 4-5 shows the respective mean sizes to be 99 and 95 nm. However, the graph below shows that the slight decrease in size for the NPs extracted from mussel matrix is not caused by reducing the size of the refined NPs, but rather from the contribution from the natural NPs in the lower region of the size distribution at 40-50 nm.

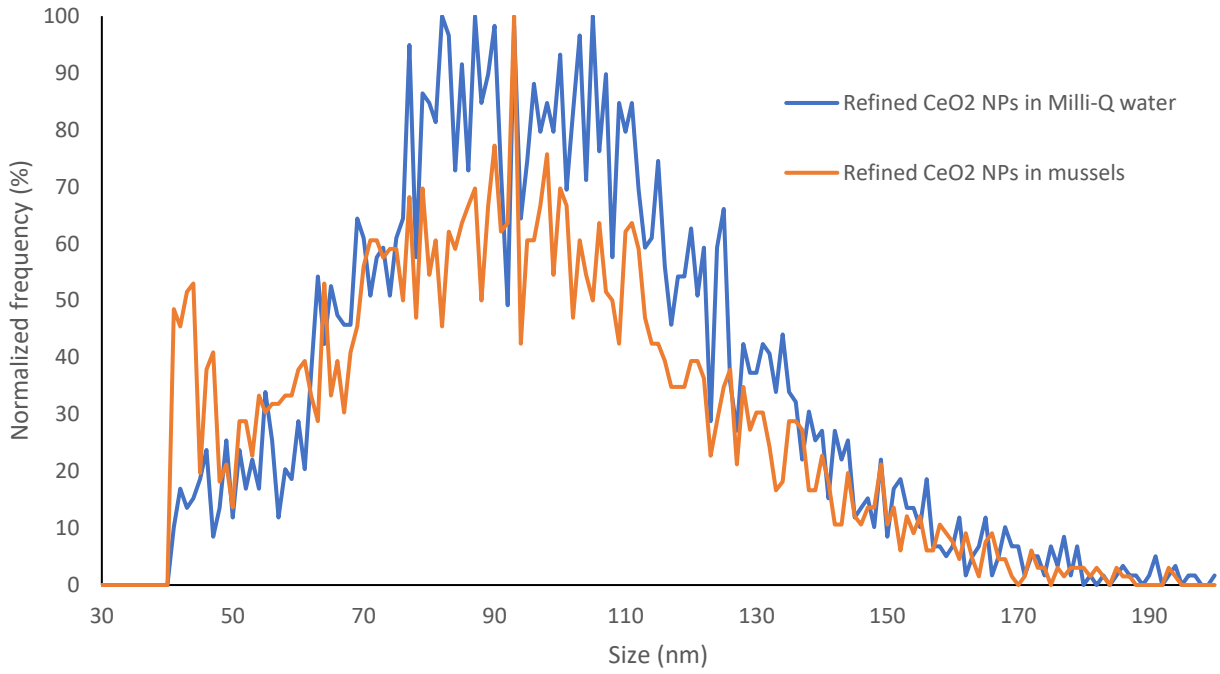

Figure 4-5: Comparison of the normalized size frequencies (%) of refined CeO_2 NPs recovered from mussel matrix and in Milli-Q® water.

Table 4-6 and **Figure** 4-6 shows the size-wise stability of the refined CeO_2 NPs by showing the mean and median sizes measured the same day as the refining and the same parameters measured after 45 days in a centrifuge tube at 4 °C. There is about a 10% decrease in the mean size after 45 days from 109 nm to 98 and a 7% decrease in median size from 105 nm to 97

Table 4-6: Mean and median sizes of newly refined CeO_2 NPs compared mean and median sizes of refined CeO_2 NPs stored for 45 days.

Sample	N	Parameter	Mean size (nm)	Median size(nm)
Freshly refined CeO_2 NPs	2	Mean	109	105.0
Refined CeO_2 NPs after 45 days	2	Mean	98	97

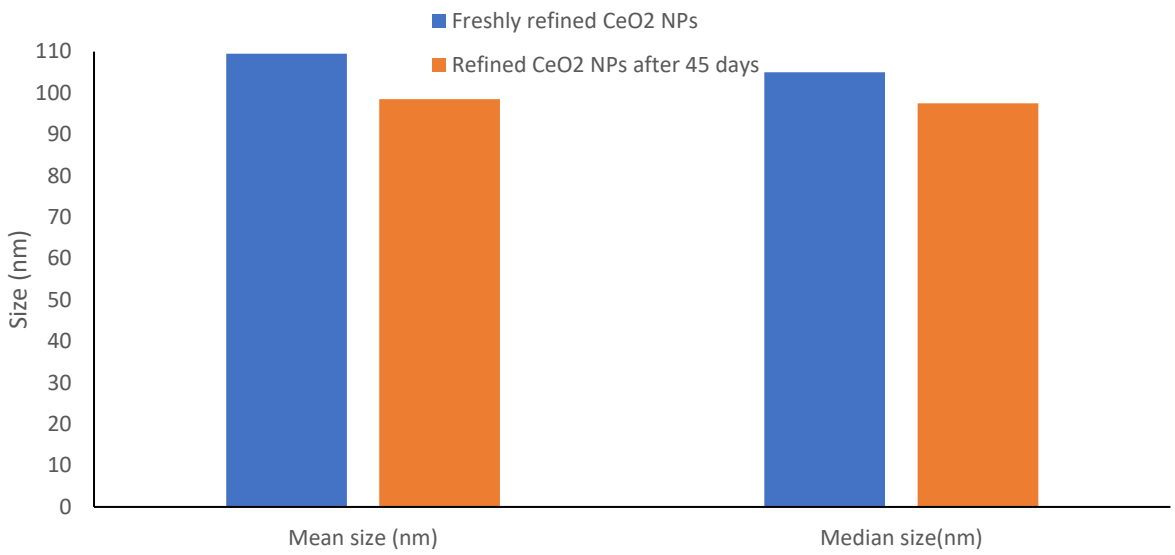

Figure 4-6: Size comparison for stability assessment.

Figure 4-7 shows the normalized size frequencies of fresh refined (orange) and stored (blue) CeO_2 NPs. There is a difference of 10 nm in the PDT from 20 to 30 nm for stored and fresh NPs, respectively. The impact of the smallest particles is small relative to larger particles. As the particles in this region only counts for about 10% of the particles measured, the difference in PDT is assumed not to have a significant contribution in the size decrease calculation in the MH software.

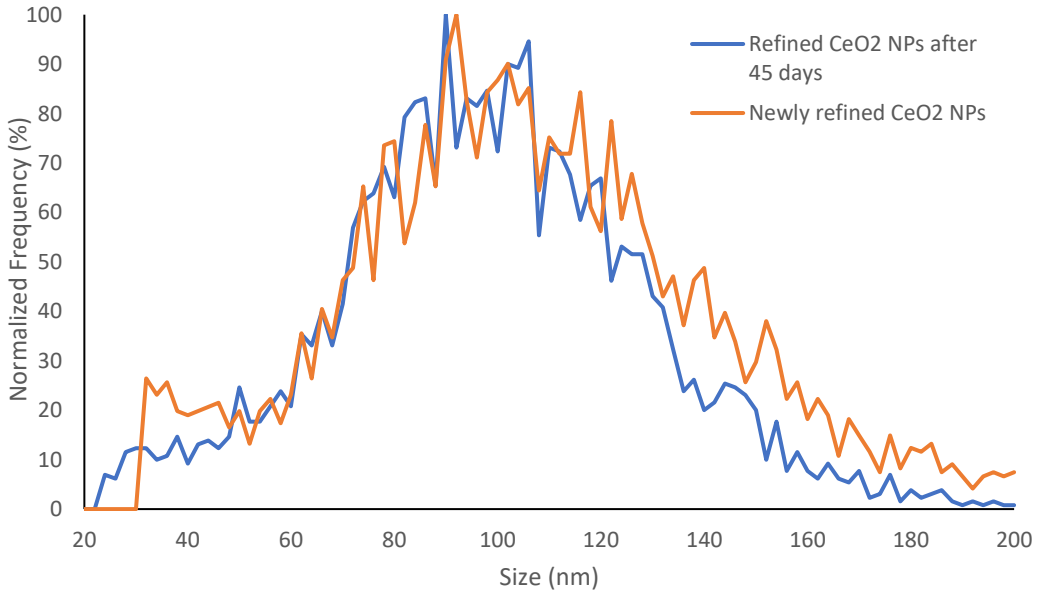

Figure 4-7: Normalized size frequency of newly refined CeO_2 NPs compared to the same particles after being stored for 45 days.

4.1.4 Titanium dioxide < 150 nm nanoparticles

Table 4-7 shows the results from the extraction- recovery analysis of unrefined TiO_2 NPs spiked in cod matrix. When adjusted for the natural contribution, the recoveries for particle number and mass concentration were found to be 46% and 534%, respectively. The recovery of the FullQuant concentration was also found to be extremely high and can most likely be explained by the contribution of TiO_2 in the Protamex® powder. This can also be the reason for the high variation in sizes between TiO_2 NPs in Milli-Q® water and recovered TiO_2 NPs after enzymatic where the sizes are calculated to be 42 and 63 nm, respectively.

Table 4-7: Results from the extraction- recovery analysis of unrefined TiO_2 NPs spiked in cod matrix.

Samples	N	Parameter	Particle number	Mass conc. (ng/L)	FullQuant conc. (ng/L)	Mean size (nm)	Median size (nm)
TiO_2 NPs 70 ng/L in Milli-Q® water	3	Mean	3660	21	20	42	39
		Min-max	3546 - 3852	19-22	19-21	42-42	39-39
		RSD (%)	4.6	6.7	3.5	5.7	4.4
TiO_2 NPs in cod samples	2	Mean	2629	44	122	50.5	43
		Min-max	2299 - 2959	36-52	118-127	50-51	50-52
TiO_2 NPs in spiked cod samples	4	Mean	4304	154	196	62	54
		Min-max	3804 - 5370	136-174	190-217	58-65	58-66
		RSD (%)	16.8	13.5	13.4	5.1	2.6
		Recovery (%)	46	523	370	149	138

4.1.5 Centrifuged titanium dioxide nanoparticles

Table 4-8 shows the results from the analysis of a suspension from each step in the refinement process of TiO_2 <150 nm NPs, including before the process started (times centrifuged = 0). A steady increase in the size-parameters is observed, from 42 nm to 88 nm in mean size. As mentioned in chapter 3.5.2, the dilution of the suspensions was done with respect to the particle number as this is a tangible approach to quickly assess further dilution. A particle number between 1000 – 4000 was assessed to be optimal. The dilution after the first cycle was not optimal as the instrument detects 7648 NPs, however the data does not seem to be too affected by this matter. After mass concentration after the first and third cycle are almost equal at 71.7 and 71.2, respectively. However, after the first cycle, the suspension contains seven times the number of NPs than after the third cycle due to the increase in NP size from 48 nm to 82 nm.

The Table includes values for the extra centrifuge step explained in chapter 3.4.2. After this step, the mean and median sizes decrease 88 nm and 82 nm to 76 and 70 nm, respectively.

Table 4-8: Stepwise results of number and mass concentration and mean, median and most frequent sizes during the refinement procedure of TiO_2 <150 nm NPs

Times centrifuged	Particle number	Mass conc. (ng/L)	FullQuant conc. (ppb)	Mean size (nm)	Median size (nm)	Most frequent size
0	2377	14.6	0.032	42	39	30
1	7648	71.7	0.056	48	45	40
2	1586	61.1	0.039	71	64	57
3	1247	71.2	0.045	82	74	73
4	1102	63.7	0.040	85	77	66
5	1333	88.0	0.055	88	82	63
6*	1419	56.7	0.036	76	70	58

***** Extra step included to eliminate accumulation of larger particles. See **Figure** 4-9.

Figure 4-8 shows the particle size distribution from steps 0-5 in the process of refining TiO_2 <150 nm NPs. The top left gives the distribution of the unrefined NPs where most of the particles are in the lower region of the detectable size range, from 30-50 nm. After two completed cycles, the median size has shifted from 39 nm to 64 nm. A small accumulation of larger NPs between 120-160 nm is observed. Although most of the NPs are relatively evenly distributed in a gaussian-like shape stretching from 30 to 120 nm, the secondary top also increases in size from steps 3 to 6.

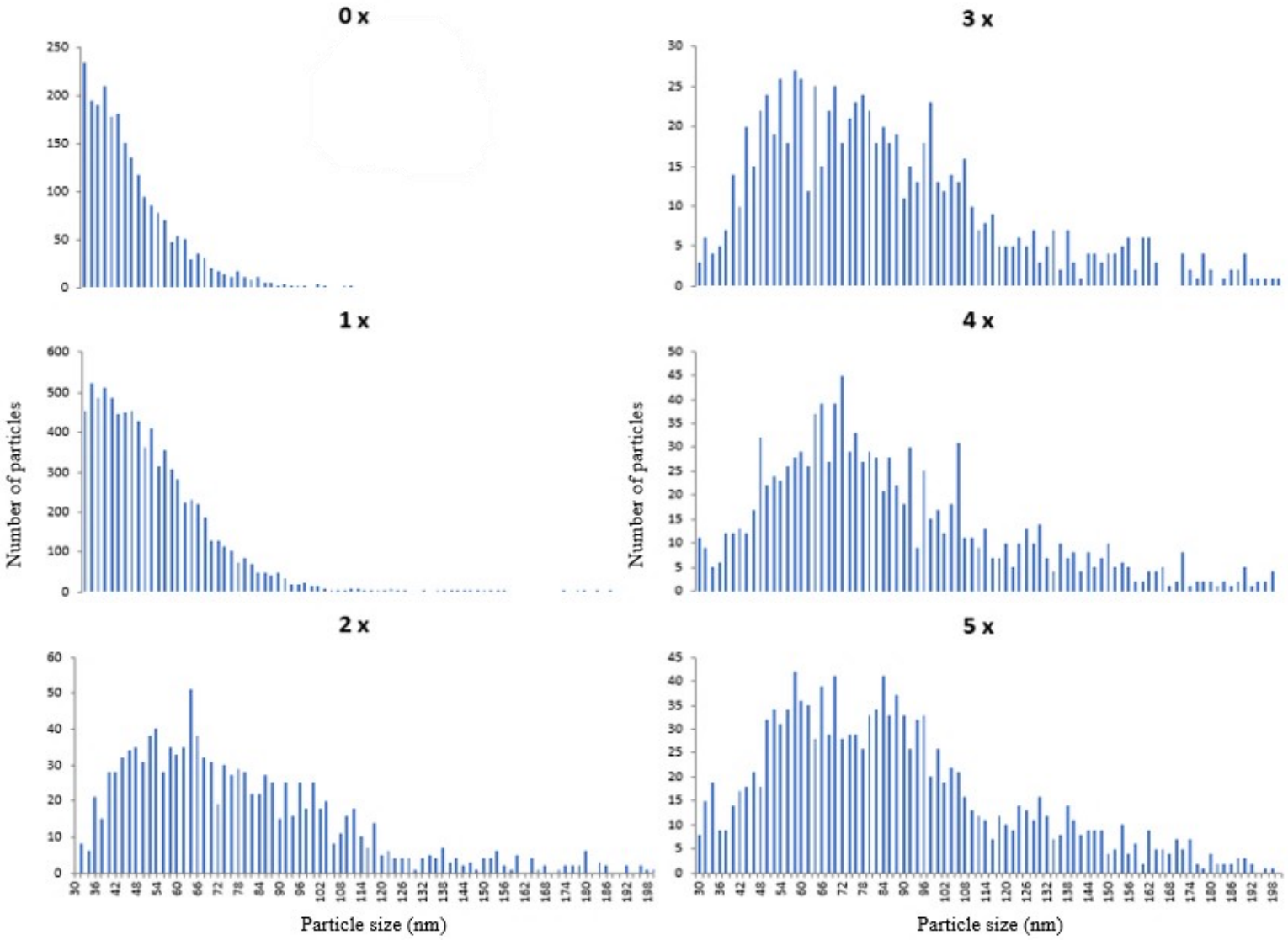

Figure 4-8: The stepwise overview of the particle size distribution during the refinement process for TiO_2 < 150 nm NPs

As mentioned in chapter 3.4.2, an extra step in the refining process (step 6 in **Table** 4-8) was implemented as an attempt to smooth the distribution by discarding the largest particles after centrifuging the suspension. The results from this step is shown in **Figure** 4-9. The shape of the distribution is still holding a longer tail on the right side, but a decrease of the accumulated NPs between 120 nm and 160 nm is observed.

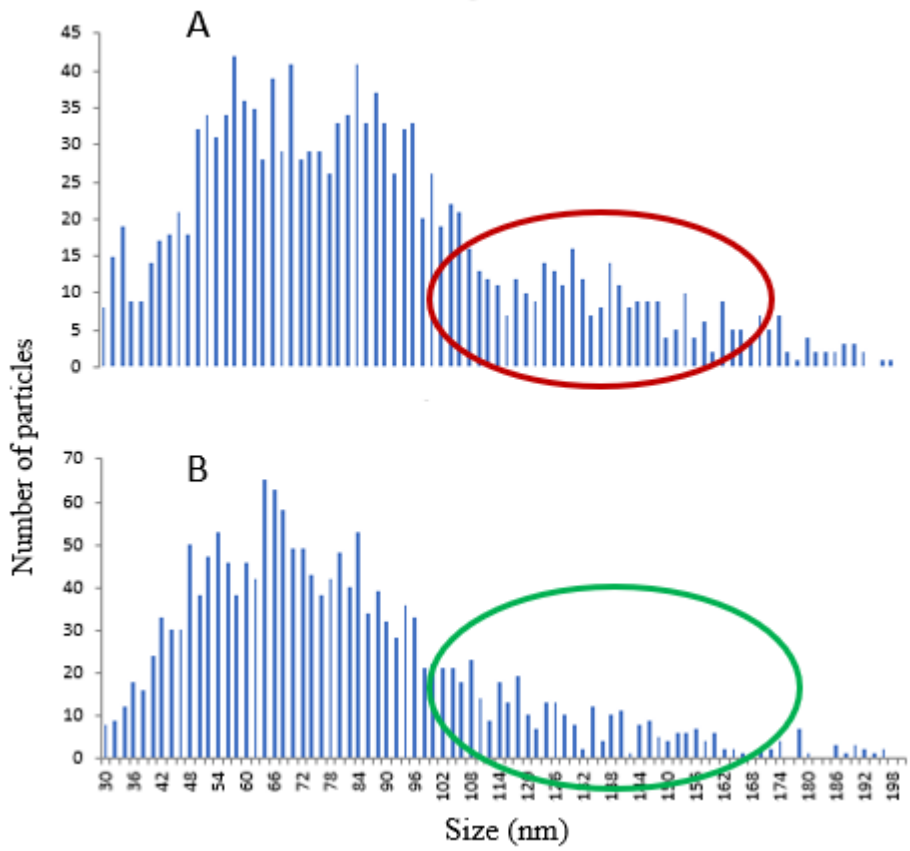

Figure 4-9: Size distributions of the refined TiO_2 NP suspension before (A) and after (B) the extra centrifuging.

Table 4-9 shows the results for spike-recovery analysis of refined TiO_2 NPs in cod matrix. The Table also includes results from analysis of natural contribution from mussels as well as refined TiO_2 NPs in Milli-Q® water as the theoretical reference. When adjusted for contribution of TiO_2 NPs in the cod matrix and Protamex® solution, the particle number and mass concentration recoveries were found to be 71% and 112%, respectively. The recoveries of the particle concentration and the FullQuant concentration were 71% and 113%, respectively. The mean and median sizes of the NPs measured in unspiked cod samples were analyzed to 61.5 nm and 50 nm, respectively, while the mean and median sizes refined TiO_2 NPs spiked and recovered from cod matrix were found to be 104% and 83%, respectively. The threshold was in this case set to 40 nm.

Table 4-9: Mean values, RSDs and recoveries of particle numbers, particle concentrations, mass concentrations, FullQuant concentrations and sizes of refined TiO_2 NPs spiked in cod matrix with enzymatic digestion and in Milli-Q® water.

Samples	N	Parameter	Particle number	Particle conc. (par/L)	Mass conc. (ng/L)	FullQuant conc. (ng/L)	Mean size (nm)	Median size (nm)
Refined TiO_2 NPs in Milli-Q® water	4	Mean	2581	$7.3x10^7$	215.5	133	91	83
		Min-max	2207-3026	6.2-8.5($x10^7$)	170-281	103-172	90-93	81-84
		RSD (%)	13.4	13.4	22.0	22.2	1.4	1.5
Natural TiO_2 NP in cod samples	2	Mean	113	$3.20\ x10^6$	4.0	40.5	61.5	50
		Min-max	85-142	2.4-4.0 ($x10^6$)	3.4-4.7	36-45	61-62	50-50
TiO_2 in spiked cod samples	4	Mean	1960	$5.50\ x10^7$	246.5	191.0	95	83.
		Min-max	1933-2026	5.4-5.7 ($x10^7$)	211-266	166-218 ($x10^7$)	94-97	82-84
		RSD (%)	2.2	2.5	13.7	12.2	1.5	0.9
		Recovery (%)	71	71	112	113	104	100

Figure 4-10 shows the normalized size distribution of refined TiO_2 NPs recovered from spiked cod matrix and the normalized distribution of the same particles in Milli-Q® water without any biological matrix or enzymatic digestion routine. There is no obvious difference between the two distributions in the Figure to be observed, other than a slightly higher portion of the NPs in cod matrix are in the region of 50-60 nm, due to the contribution of TiO_2 in cod matrix and Protamex® solution. **Table** 4-9 shows that the median size for NPs in cod matrix and Milli-Q® water are practically equal at 83 nm, but the mean size for refined NPs in cod is slightly larger for refined NPs in Milli-Q® water at 95 nm and 91.5 nm, respectively.

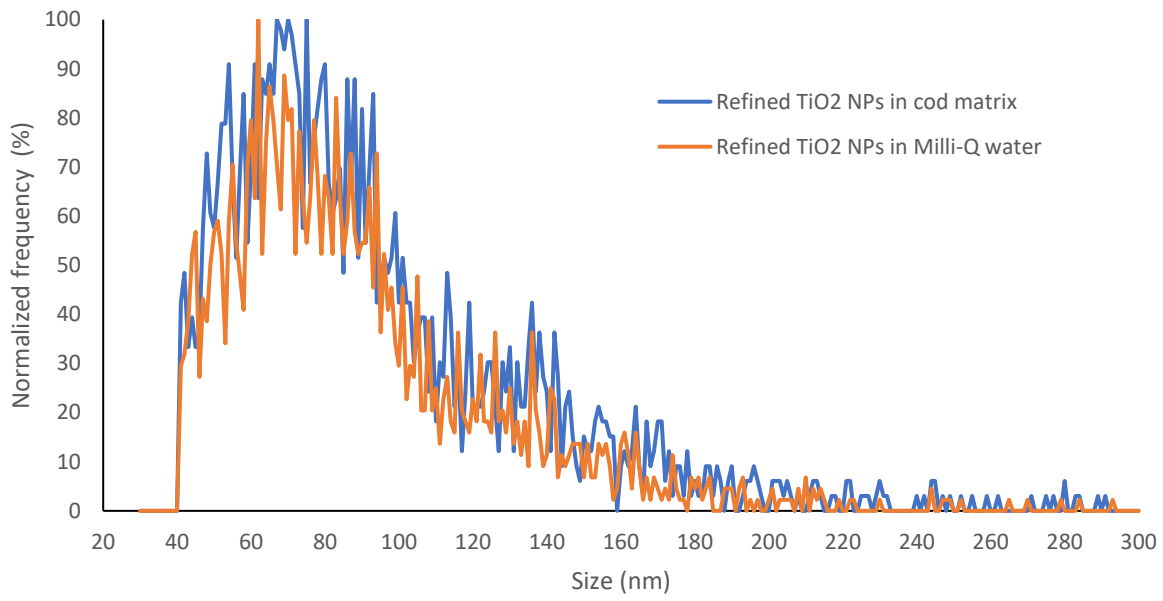

Figure 4-10: Comparison of refined TiO_2 NPs Milli-Q® water and the same particles extracted from cod matrix after enzymatic digestion.

In **Table** 4-10, **Figure** 4-11 and **Figure** 4-12 shows the results after testing the stability of the refined TiO_2 NPs. both the mean and median sizes increase noticeably from 80 nm to 90 nm and from 73 nm to 82 nm, respectively. The normalized size distributions in **Figure** 4-12 do not differ significantly, but the top of the curve of the stored NPs are wider and the entire distribution of the stored NPs is shifted slightly towards larger sizes.

Table 4-10: Mean and median sizes fresh and stored refined TiO_2 NPs.

Sample	N	Mean size (nm)	Median size (nm)
Freshly refined TiO_2 NPs	1	80	73
Refined TiO_2 NPs after 20 days	1	90	82

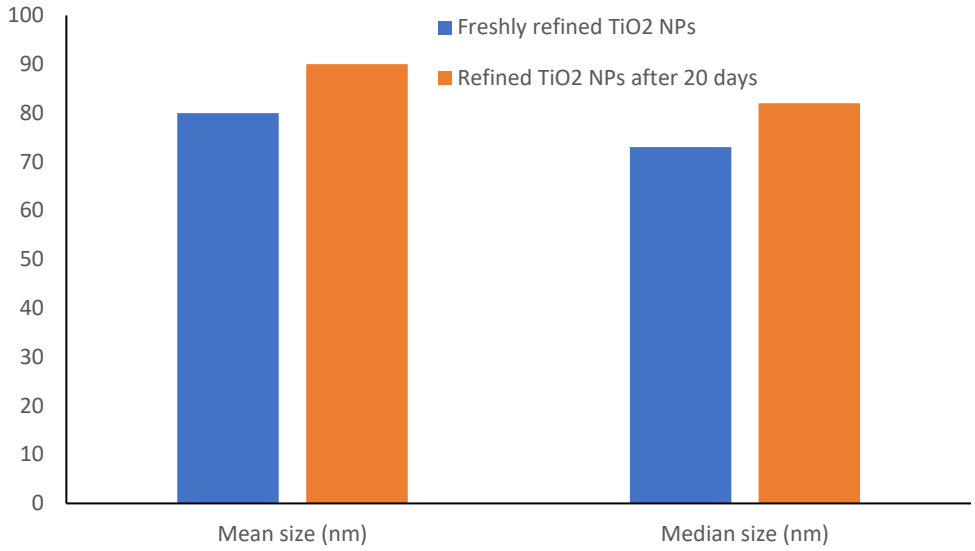

Figure 4-11: Histogram comparing mean and median sizes of newly refined TiO_2 NPs and the same NPs after being stored for 20 days.

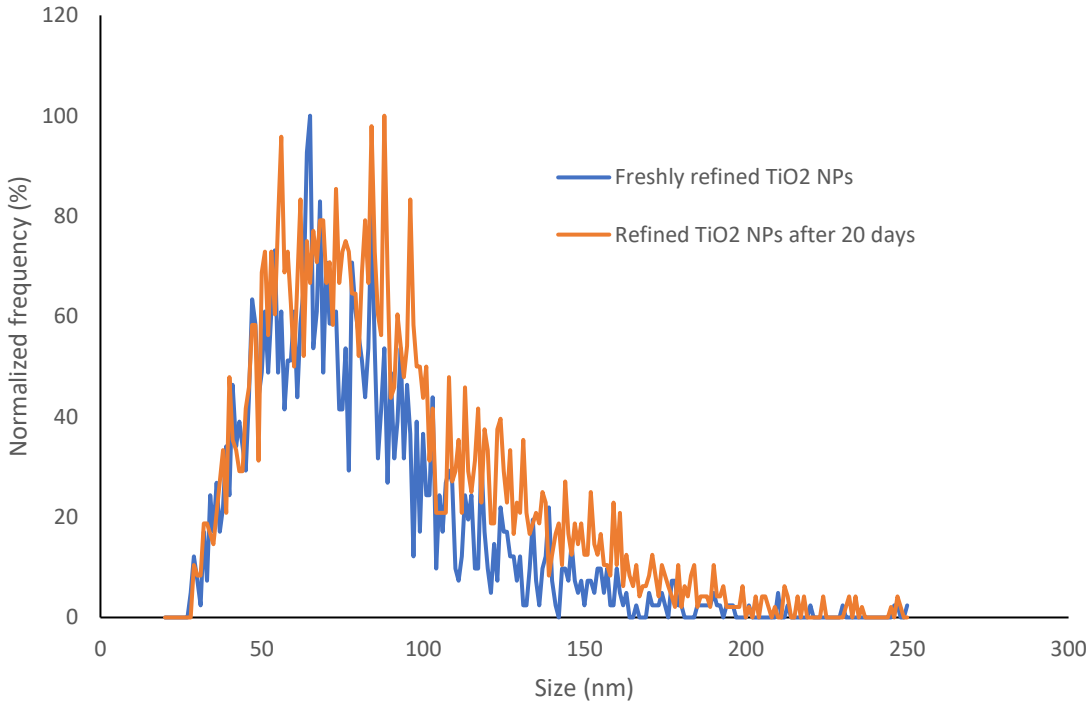

Figure 4-12: Comparison of the normalized size distributions of newly refined TiO_2 NPs and the same NPs after being stored for 20 days.

4.2 Scanning Electron Microscopy (SEM)

All SEM-analyses were performed on a Zeiss Supra 55VP instrument on UoB`s facilities with the help of Irene Heggstad (UoB).

4.2.1 Gold 60 nm nanoparticles

The SEM analysis of 60 nm gold nanoparticles (**Figure** 4-13 and **Figure** 4-14) revealed the shape and size to be relatively spherical and monodisperse, although varying to some degree. The NPs in the red rectangle in **Figure** 4-13 marks the Au NPs included in the analysis of size distribution in ImageJ. Measurements performed with ImageJ-software shows a span between 50-70 nm of the measured particles, where most of the particles are between 60-64 nm in diameter (**Figure** 4-15).

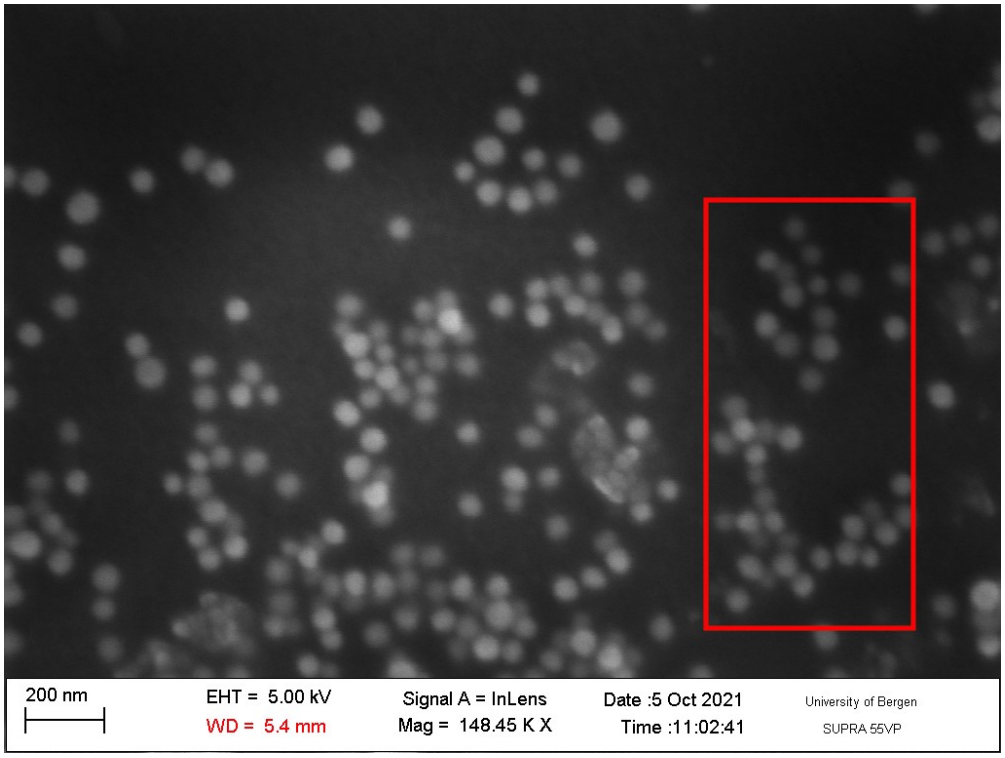

Figure 4-13: SEM analysis of 60 nm gold nanoparticles from NanoComposix (Zeiss Supra 55 VP). In red rectangle: Particles measured with ImageJ.

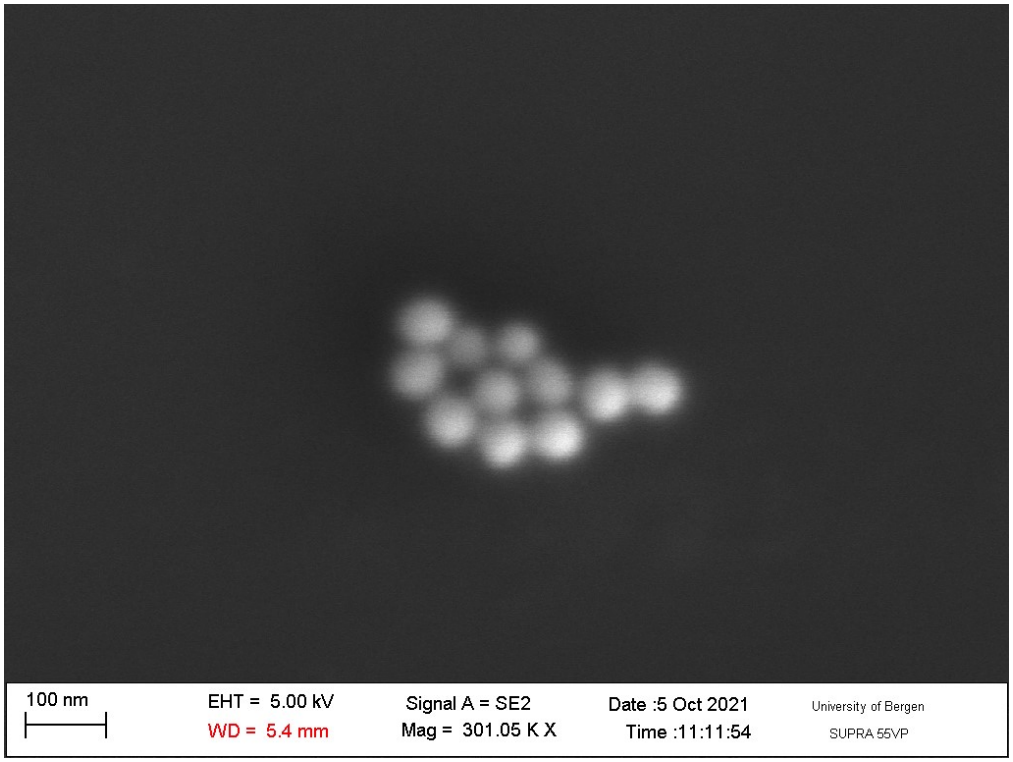

Figure 4-14: SEM analysis of 60 nm gold nanoparticles from NanoComposix.

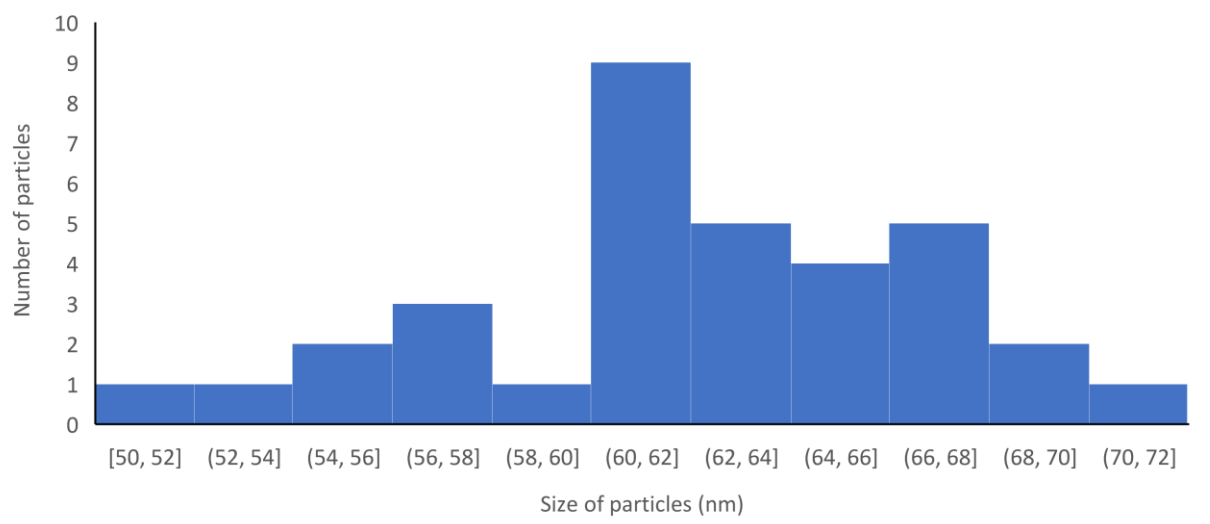

Figure 4-15: Size distribution histogram of 60 nm Au NPs from NanoComposix, analysed with SEM and measured in ImageJ. (N=34. Mean size = 62 nm)

4.2.2 Cerium dioxide nanoparticles

SEM analysis of unrefined CeO_2 NPs (**Figure** 4-16) shows irregularity with large variations in the size and shape of the particles. Many of the particles are in the size range of 30-50 nm in at least one external dimension, but a substantial amount of the particles is even smaller, and some are much larger. With ImageJ software, some of the particles were measured to over 200 nm. The low image quality due to unknown instrumental causes made it impossible to perform a general size-distribution analysis with ImageJ, as the particles below 20 nm could not be accurately measured by the software.

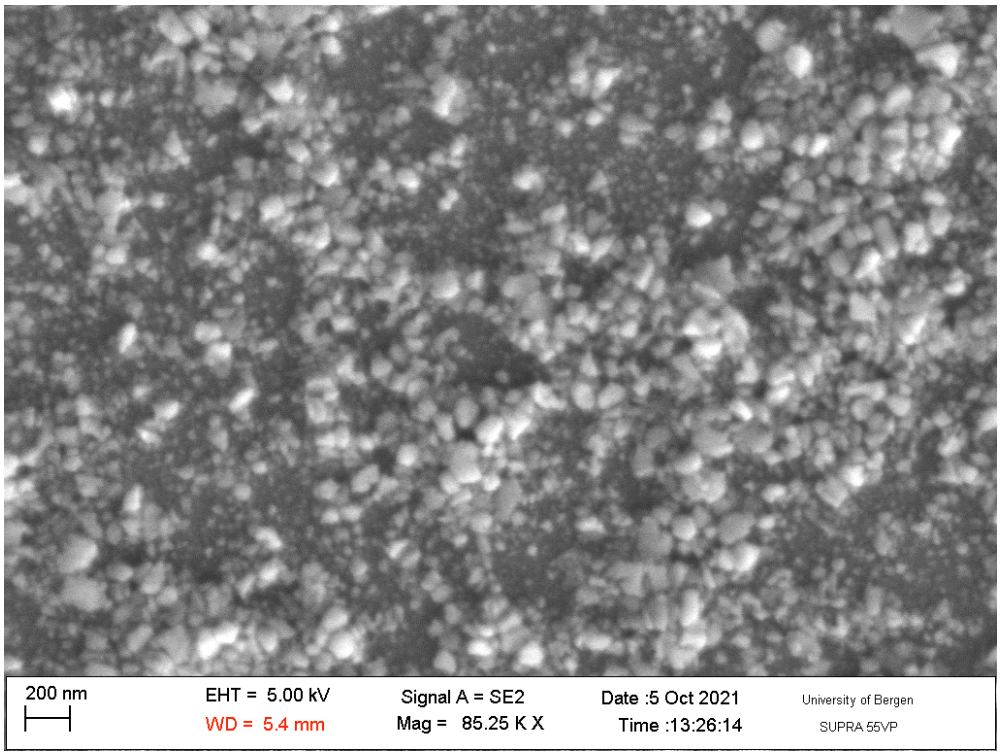

Figure 4-16: SEM analysis of CeO2 NPs (30-50 nm) before the refinement process.

The SEM analysis of the refined CeO_2 NPs in **Figure** 4-17**Figure** 4-16 shows a higher regularity in the size distribution of the particles compared to before refinement process. Size measurements of the CeO_2 NPs performed with ImageJ (**Figure** 4-18) gives a span between 33-208 nm in diameter, where most of the particles are in the range of 60-130 nm, approximately.

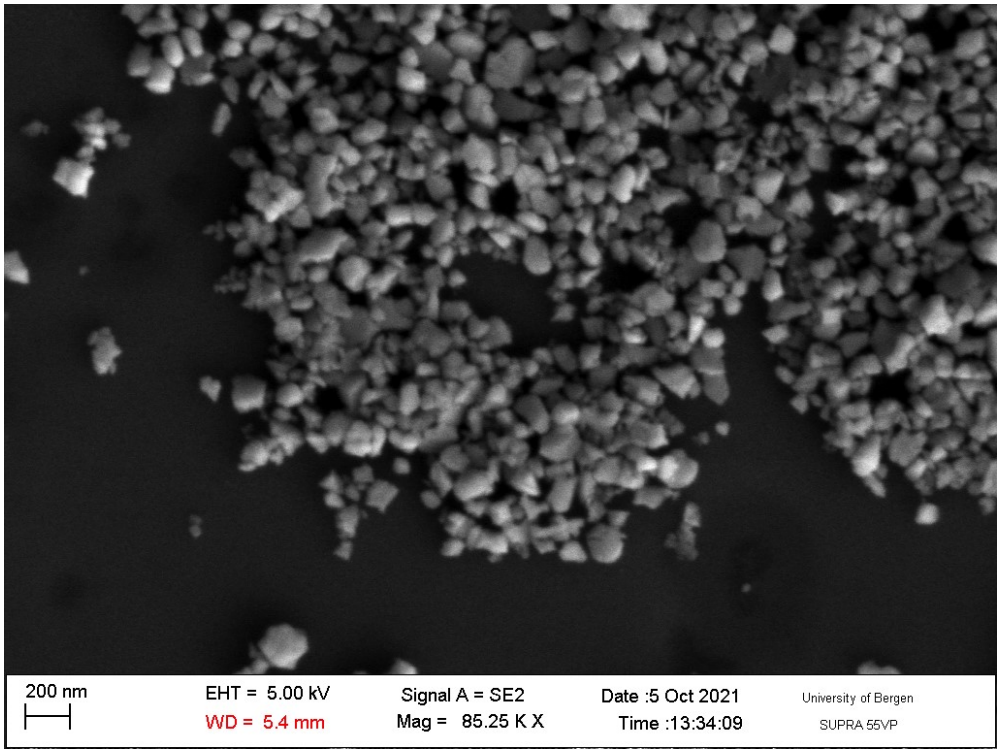

Figure 4-17: SEM analysis of CeO_2 NPs (30-50 nm) after refinement process.

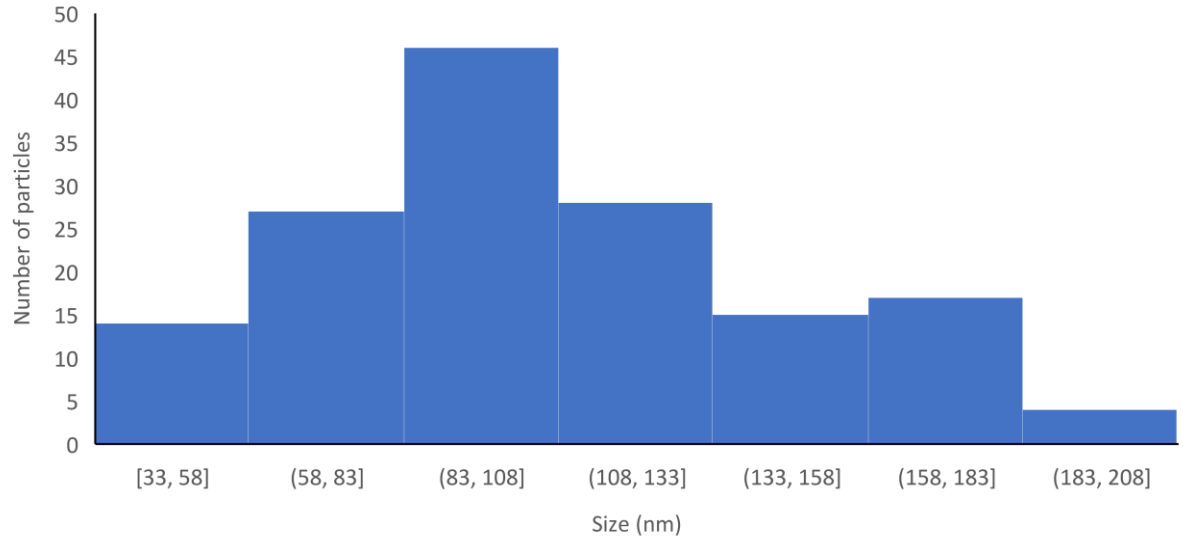

Figure 4-18: Size distribution histogram of refined CeO_2 NPs. Analyzed with SEM and measured with ImageJ. N = 151. Mean size = 107 nm.

4.2.3 Titanium dioxide nanoparticles

Figure 4-19 and **Figure** 4-20 shows the results of SEM analysis of unrefined and refined TiO_2 NPs. The quality of the images is not optimal due to unknown instrumental causes. For the SEM analysis of unrefined TiO_2 NPs (**Figure** 4-19) the concentration of the analyte suspension

looks to be higher than optimal, an inconvenience when assessing the sizes of the NPs. Although a notable difference in the SEM analysis of the two suspensions is observed, the images does not provide sufficient basis of comparison with the sp-ICP-MS results.

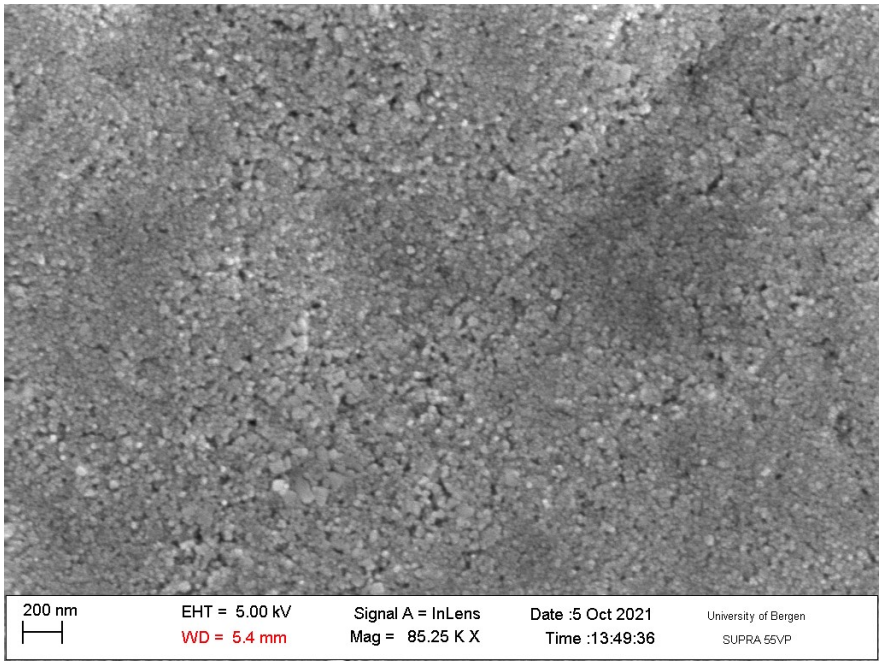

Figure 4-19: SEM image of TiO_2 <150 nm NPs before the refinement process.

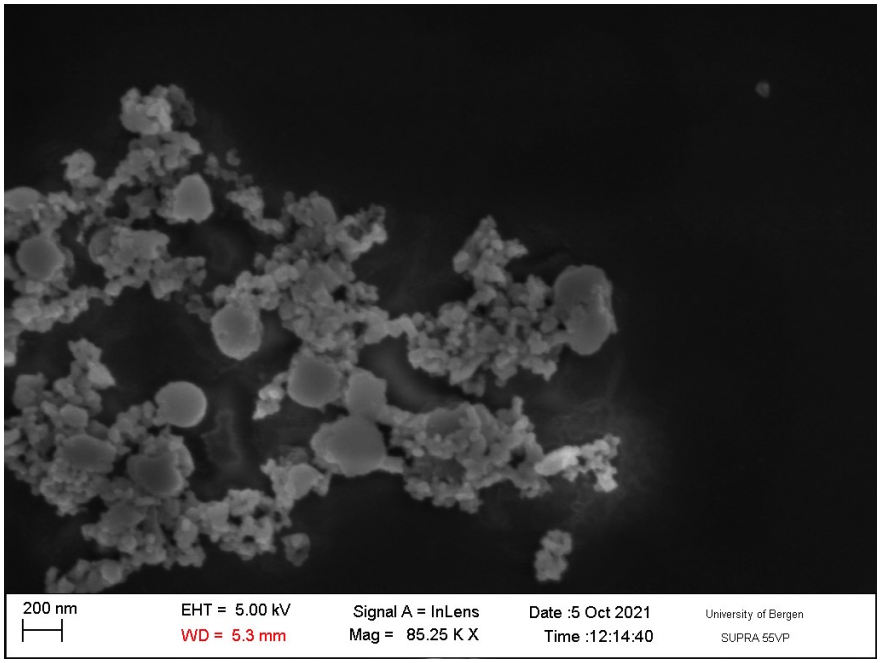

Figure 4-20: SEM image of refined TiO_2 NPs.

5. Discussion

5.1 Au 60 nm nanoparticles

Au 60 nm NPs were used as a reference material, to determine the NE as well as a complimentary material in the recovery analysis of CeO_2 and TiO_2 in mussel and cod, respectively. Au NPs was found to obtain suitable properties for functioning as a reference material. NE were stable between 5-6% throughout all the analysis and had overall miniscule variations in other parameters. The low background, lack of interference, and optimal separation between NP signal and background signal, laid the basis for robust analysis and high reproducibility.

The recovery analysis of Au 60 nm NPs in cod and mussels found the recovery of particle number and mass concentration to be lower than expected when comparing results with the validated method from IMR [5] (**Figure** 4-1). This applies to both mussel and cod matrix. With mussels, the Au analysis was executed after the analysis of CeO_2 recovery, meaning that CeO_2 and Au NPs were spiked at the same time, but the CeO_2 analysis was ran to a completion, before starting a new sequence with Au analysis about 3-4 hours later, without stirring or shaking the centrifuge tubes in between. For cod, the analysis of spiked Au and TiO_2 NPs was executed in multielement mode which means multiple elements can be measured in one sample uptake. In reality, only one isotope is measured at a time, but the mode allows for switching between different configurations, quadrupole modes, and target isotopes during one sample uptake. Therefore, the analysis time of one single sample can be very time-consuming in multielement mode.

The prolonged time between spiking and analyzing is likely the reason for the low recovery of Au NPs in both cases. Time is of the essence, as NPs can agglomerate, sink, and adhere to surfaces as time goes by. The validation tests were performed with more optimal, less time-consuming conditions. As a substantiating argument, the size of the recovered Au NPs have not decreased, meaning that the low recovery is not caused by dissolution.

5.2 Work-up and analysis of CeO_2 nanoparticles

5.2.1 Unrefined CeO_2 30-50 nm nanoparticles

Untreated CeO_2 NPs were diluted and analyzed with theoretical concentrations of 100 ng/L and 200 ng/L, which gave measured concentrations of 62 ng/L and 111 ng/L, respectively.

Although this is lower the expected, the results agree with earlier analysis of the same material at IMR. [24] The low concentrations can be explained by various reasons such as agglomeration, surface adsorption, and/or dissolution. CeO_2 NPs are known for their low solubility [29] and the most likely explanation comes from the small size of many of the particles in the untreated stock suspension, judging by the shape of the size distribution on the top left of **Figure** 4-3.

The PDT is set at 25 nm, which also is close to the most frequent size detected. The slight dip in the frequency near the PDT is not an indication of a lower number of particles on the left side of the highest peak, it appears as a result of "slicing" the relevant size-bin at the PDT; the bars are affiliated a specific bin size which is set at 1 nm by default. This means that if the PDT is set at 20.7 nm, only those NPs from 20.8 nm and above will be included in the bar that shows 20 nm NPs, which can give the impression that there is a larger number of NPs at 21 rather the 20, although this might not be the case. The polydispersity is high, and the actual size distribution is not possible to account for by the relevant sp-ICP-MS system due to the overlap between background an NP signal (signal/noise ratio) as the sizes get smaller.

5.2.2 Refined CeO_2 nanoparticles

Two different methods were used to refine the CeO_2 NPs: With and without probe sonication after the centrifuging in each cycle of the refinement process. **Table** 4-4 suggests that the preferred method should be to not sonicate the samples based on the increased RSD of the measurements of sonicated samples. However, one positive aspect of sonicating the samples is the assurance of complete dissolution of any potential agglomerates formed in the centrifuge. More time and effort must be considered when only relying on shaking by hand and by vortex shaking. On the other hand, the use of sonication treatments demands consistent application across laboratories, as probe sonication and other sonication methods can alter the physical and chemical properties of nanomaterials [30] by for instance reducing the size distribution or induce agglomeration. The use of sonication should therefore always be avoided if possible. Thus, the non-sonicated method was used further in this project.

The refined product has a completely different size distribution than the starting suspension. Where untreated NPs has a gradually transition between noise signals and particle signals in the MH software, the NP signals of the refined product has a clear distinction between the two, leading to simplification in determining the correct position of the PDT, less subjected to

human bias. The number-recovery of refined NPs in mussel matrix (**Table** 4-5) was found to be 78% with an RSD value of 2.2%, suggesting that some of the particles will adsorb on the surface of the inside of the centrifuge tubes. The mean diameter of the recovered CeO_2 NPs obtains a lower mean diameter of 94 nm compared to 99 nm in Milli-Q® water. This is likely to be caused by a signal suppressing matrix effect [31]. The SEM images of CeO_2 NPs (chapter 4.2.2) are of mediocre quality, but still shows consistency with the results from sp-ICP-MS. The most important observation from the images is the removal of smaller particles when comparing images of refined and unrefined NPs.

5.3 Work-up and analysis of TiO_2 nanoparticles

As mentioned in chapter **3.3**, an adjustment in the enzymatic digestion procedure in analysis of TiO_2 was made as an attempt to minimize the high background observed in preliminary tests. First, the biological test matrix had to be changed to cod, as filter feeders like mussels which lives near the coastline, contains substantial amounts of particulate TiO_2 and dissolved Ti, thus making mussels as a sample matrix unusable. Further tests showed that the Protamex® solution also contributed to a significant increase in the amount of TiO_2 found in the digested samples. Qonsequently, the concentration of Protamex® was decreased from 20% to 2%. To make up for the lowered enzyme concentration, the incubation time was increased from 1 hour to 18 hours.

5.3.1 Unrefined TiO_2 <150nm nanoparticles

The unrefined TiO_2 NPs were diluted and analyzed in Milli-Q® water with a theoretical concentration of 70 ng/L. Spike-recovery analysis of unrefined TiO_2 NPs in cod matrix were also performed. **Table** 4-7 shows the results of these tests. In Milli-Q® water, the concentration was measured to 21 ng/L. The low concentration can be explained by the difficulty of handling distributions of small particles in the MH software. As explained in chapter **2.2.2**, the PDT is set based on visual interpretations of the raw signal distribution. In this analysis, the PDT was set at 30 nm. **Attachment** 1 shows the raw signal plot of the size distribution from which the PDT must be determined from. There is no clear distinction between background signals and NP signals, making it problematic to determine the position of the PDT, which subsequently makes it difficult to handle this material with respect to reproducibility, as subjective preference of signal interpretation is involved. A more aggressive position (lower position) of the PDT would give higher calculated mass concentration, but the uncertainty would increase

as well, as it becomes increasingly difficult to distinguish between background and NP signal. **Attachment** 2 gives the normalized size distribution which agrees on the assumption that a large part of the NPs is smaller than the PDT. Like the normalized CeO_2 size-distribution, a dip in frequency in the size nearest the PDT is observed. See explanation of this in chapter **5.2.1.**

Table 4-7 also includes analysis of TiO_2 in spiked and unspiked samples. The contribution of TiO_2 from unspiked samples is high. The particle number and mass concentration were analyzed to 2629 and 44 ng/L, respectively. The measured values for the particle number and mass concentration for spiked samples, was 4304 and 154 ng/L, giving a recovery of 46% and 523%, respectively. All difference between measured values for TiO_2 in cod samples and spiked cod samples should in theory be explained by the content of spiked NPs. However, the difference in the mass concentration amounts to 110 ng/L, which is extremely high compared to the theoretic value of 21 ng/L measured in Milli-Q® water. The reason for this high number is not known but is likely to be caused by systematic error. Nevertheless, this recovery analysis exemplifies the challenge of working with TiO_2, which is both omnipresent [32] and subjected to interferences when analyzed by sp-ICP-MS. The contribution of the potential instrumental error related to measuring the theoretical value (NPs in Milli-Q® water) on the day before the spike analysis is difficult to account for, as the size distribution of both natural and spiked NPs overlaps with each other and the background signal. Therefore, the reproducibility of PDT determination is low.

5.3.2 Refined TiO_2 nanoparticles

The size distribution of TiO_2 NPs <150 nm stock suspension was refined using the procedure in chapter **3.4.2**, and the stepwise change in mean, median, and most frequent size are shown in **Table** 4-8. The mean and median size increased from 42 nm to 88 nm and from 39 to 82 nm. In the refinement process it was necessary to induce pellet formation by centrifuging before any change in the size distribution was observed. This required a higher starting concentration compared to for CeO_2, as less NPs would be transferred in each step in a pellet. After the centrifuging, the pellet was impossible to dissolve by hand or vortex shaking making the use of probe sonication unavoidable in the case of TiO_2 refinement.

Figure 4-8 shows the stepwise plots of the size distributions from steps 0 to 5. The refinement process was regarded as highly successful even though an accumulation of larger particles from 120 nm to 160 was observed. The extra "reversed" refining step (explained in chapter **3.4.2**

and shown in step 6 in **Figure** 4-8 and in **Figure** 4-9) proved to be highly successful as the tail of the size distribution was nearly completely flattened, generating a more Gaussian-like shape which is favorable in potential statistical analysis. Going from refining step 5 to 6, an overall size decrease is observed, from 88 nm to 76 nm, and from 82 nm to 70 nm for the mean and median sizes, respectively. Due to the size decrease, it can be argued that the step should not be included, as the highest priority is to create the largest possible size distribution to keep the raw signals from the NPs well-separated from background signals. In this project, the final size distribution is considered good enough after the extra step, as the median size of 76 is about twice the size of the detection limit, which in this project was between 30-40 nm.

In the analysis of refined TiO_2 NPs spiked in cod matrix, the recoveries of particle number and mass concentration were found to be 71% and 112%, respectively (**Table** 4-9). The contribution of natural TiO_2 in unspiked cod samples is very low. The mean number of natural particles detected were 113, and the mass concentration were found to be 4 ng/L. In comparison, the recovery analysis of unrefined TiO_2 NPs the same gave a result of 2629 and 44 ng/L for the particle number and mass concentration, respectively. Although the actual content of TiO_2 in the cod samples are to a large degree equal, the possibility of moving the PDT allows for a more precise measurement and higher reproducibility. **Attachment** 3 shows the raw signal distribution from which the PDT was determined. The left side of the PDT (pink line) shows the background signals from electronic noise and smaller NPs from the cod matrix, while the right side shows the refine TiO_2 NPs spiked in the sample. The separation of background signals and NP signals is distinctly.

Analysis by SEM did not function as a verification method in this thesis due to the poor image quality.

6. Conclusion

During the scope of this project, TiO_2 and CeO_2 NPs have been analyzed in different matrices with various degree of success. The method of which the thesis is built on was designed for Au NPs but proved to be promising for other elements as well.

An easy method for the refining of size distributions for CeO_2 and TiO_2 NPs by using standard, readily available lab equipment was developed. The refined suspensions improved the quality of the analysis massively by giving opportunity to move the particle detection threshold away from the lower detection limit of NPs.

7. Further research

- The validated method for Au NPs in mussels, should be tested with different types of NPs and matrices
- The refining process should be further investigated as an extension of the problem related to the lack of CRMs.

8. References

[1] S. A. Bradford *et al.*, "Environmental applications and risks of nanomaterials: An introduction to CREST publications during 2018-2021," (in English), *Crit Rev Env Sci Tec,* Dec 18 2021, doi: 10.1080/10643389.2021.2020425.

[2] S. Liu and T. A.-O. Xia, "Continued Efforts on Nanomaterial-Environmental Health and Safety Is Critical to Maintain Sustainable Growth of Nanoindustry," (in eng), no. 1613-6829 (Electronic).

[3] B. Naseer, G. Srivastava, O. S. Qadri, S. A. Faridi, R. U. Islam, and K. Younis, "Importance and health hazards of nanoparticles used in the food industry," *Nanotechnology Reviews,* vol. 7, no. 6, pp. 623-641, 2018, doi: doi:10.1515/ntrev-2018-0076.

[4] F. Gottschalk and B. Nowack, "The release of engineered nanomaterials to the environment," *J Environ Monit,* vol. 13, no. 5, pp. 1145-55, May 2011, doi: 10.1039/c0em00547a.

[5] S. Valdersnes, A. M. Bienfait, B. Solli, and A. S. Bruvoll, "600 - Kalibrering av instrument for nanopartikkelbestemmelse og bestemmelse av gullnanopartikler i blåskjell med ICPMS," 2020.

[6] C. European *et al.*, *Identification of nanomaterials through measurements : points to consider in the assessment of particulate materials according to the European Commission's Recommendation on a definition of nanomaterial*. Publications Office, 2019.

[7] S. Griffin *et al.*, "Natural Nanoparticles: A Particular Matter Inspired by Nature," *Antioxidants (Basel),* vol. 7, no. 1, Dec 29 2017, doi: 10.3390/antiox7010003.

[8] N. Bastús, E. Casals, I. Ojea Jimenez, M. Varón, and V. Puntes, "The Reactivity of Colloidal Inorganic Nanoparticles," 2012, p. 24.

[9] C. de Mello Donegá, *Nanoparticles : Workhorses of Nanoscience*, 1st ed. Berlin, Heidelberg: Springer Berlin Heidelberg : Imprint: Springer,, 2014, pp. 1 online resource (XII, 299 pages 140 illustrations, 53 illustrations in color.

[10] E. Roduner, "Size matters: why nanomaterials are different," (in English), *Chem Soc Rev,* vol. 35, no. 7, pp. 583-592, 2006, doi: 10.1039/b502142c.

[11] N. Kumar and S. Kumbhat, *Essentials in nanoscience and nanotechnology*. Hoboken, New Jersey: Wiley, 2016, pp. xviii, 470 pages.

[12] P. P. Fu, Q. Xia, H. M. Hwang, P. C. Ray, and H. Yu, "Mechanisms of nanotoxicity: generation of reactive oxygen species," *J Food Drug Anal,* vol. 22, no. 1, pp. 64-75, Mar 2014, doi: 10.1016/j.jfda.2014.01.005.

[13] S. Kawanishi, Y. Hiraku, M. Murata, and S. Oikawa, "The role of metals in site-specific DNA damage with reference to carcinogenesis," *Free Radic Biol Med,* vol. 32, no. 9, pp. 822-32, May 1 2002, doi: 10.1016/s0891-5849(02)00779-7.

[14] J. Zhang *et al.*, "ROS and ROS-Mediated Cellular Signaling," *Oxid Med Cell Longev,* vol. 2016, p. 4350965, 2016, doi: 10.1155/2016/4350965.

[15] M. Valko, C. J. Rhodes, J. Moncol, M. Izakovic, and M. Mazur, "Free radicals, metals and antioxidants in oxidative stress-induced cancer," *Chem Biol Interact,* vol. 160, no. 1, pp. 1-40, Mar 10 2006, doi: 10.1016/j.cbi.2005.12.009.

[16] H. M. Bolt, R. Marchan, and J. G. Hengstler, "Nanotoxicology and oxidative stress control: cutting-edge topics in toxicology," (in English), *Arch Toxicol,* vol. 86, no. 11, pp. 1629-1635, Nov 2012, doi: 10.1007/s00204-012-0953-9.

[17] J. Jiang, G. Oberdorster, A. Elder, R. Gelein, P. Mercer, and P. Biswas, "Does nanoparticle activity depend upon size and crystal phase?," (in English), *Nanotoxicology,* vol. 2, no. 1, pp. 33-42, 2008, doi: 10.1080/17435390701882478.

[18] J. n. Blasco and I. Corsi, *Ecotoxicology of nanoparticles in aquatic systems*. Boca Raton: CRC Press/Taylor & Francis Group, 2019, pp. v, 270 pages.

[19] U. Voellkopf, M. Paul, and E. R. Denoyer, "Analysis of Solid Samples by Icp-Mass-Spectrometry," (in English), *Fresen J Anal Chem,* vol. 342, no. 12, pp. 917-923, Apr 1992, doi: Doi 10.1007/Bf00322827.

[20] P. B. Farnsworth and R. L. Spencer, "Ion sampling and transport in Inductively Coupled Plasma Mass Spectrometry," (in English), *Spectrochim Acta B,* vol. 134, pp. 105-122, Aug 1 2017, doi: 10.1016/j.sab.2017.06.009.

[21] A. technologies. *MassHunter Workstation Single Nanoparticle Application*. (2017).

[22] M. D. Montano, J. W. Olesik, A. G. Barber, K. Challis, and J. F. Ranville, "Single Particle ICP-MS: Advances toward routine analysis of nanomaterials," *Anal Bioanal Chem,* vol. 408, no. 19, pp. 5053-74, Jul 2016, doi: 10.1007/s00216-016-9676-8.

[23] R. Peters *et al.*, "Single particle ICP-MS combined with a data evaluation tool as a routine technique for the analysis of nanoparticles in complex matrices," (in English), *J Anal Atom Spectrom,* vol. 30, no. 6, pp. 1274-1285, 2015, doi: 10.1039/c4ja00357h.

[24] A. C. Kjærvik, "Metodeutvikling for bestemmelse av metallog metalloksid-nanopartikler i det marine miljø med sp-ICP-MS," M.Sc, Department of chemistry, University of Bergen, 2021.

[25] J. E. Castle and P. A. Zhdan, "Characterization of surface topography by SEM and SFM: Problems and solutions," (in English), *J Phys D Appl Phys,* vol. 30, no. 5, pp. 722-740, Mar 7 1997, doi: Doi 10.1088/0022-3727/30/5/004.

[26] J. Roma, A. R. Matos, C. Vinagre, and B. Duarte, "Engineered metal nanoparticles in the marine environment: A review of the effects on marine fauna," (in English), *Mar Environ Res,* vol. 161, Oct 2020, doi: 10.1016/j.marenvres.2020.105110.

[27] M. W. L. Popp and H. L. Ploegh, "Making and Breaking Peptide Bonds: Protein Engineering Using Sortase," (in English), *Angew Chem Int Edit,* vol. 50, no. 22, pp. 5024-5032, 2011, doi: 10.1002/anie.201008267.

[28] F. R. A. C. C. O. P. A. C. MEDICINE. "Centrifugation Parameters Calculator." http://vesicles.niifhm.ru/ (accessed.

[29] J. T. Dahle, K. Livi, and Y. Arai, "Effects of pH and phosphate on CeO2 nanoparticle dissolution," (in English), *Chemosphere,* vol. 119, pp. 1365-1371, Jan 2015, doi: 10.1016/j.chemosphere.2014.02.027.

[30] J. S. Taurozzi, V. A. Hackley, and M. R. Wiesner, "Ultrasonic dispersion of nanoparticles for environmental, health and safety assessment - issues and recommendations," (in English), *Nanotoxicology,* vol. 5, no. 4, pp. 711-729, Dec 2011, doi: 10.3109/17435390.2010.528846.

[31] C. Agatemor and D. Beauchemin, "Matrix effects in inductively coupled plasma mass spectrometry: A review," (in English), *Anal Chim Acta,* vol. 706, no. 1, pp. 66-83, Nov 7 2011, doi: 10.1016/j.aca.2011.08.027.

[32] C. Y. Yin *et al.*, "TiO2 particles in seafood and surimi products: Attention should be paid to their exposure and uptake through foods," (in English), *Chemosphere,* vol. 188, pp. 541-547, Dec 2017, doi: 10.1016/j.chemosphere.2017.08.168.

9. Attachments

Attachment 1

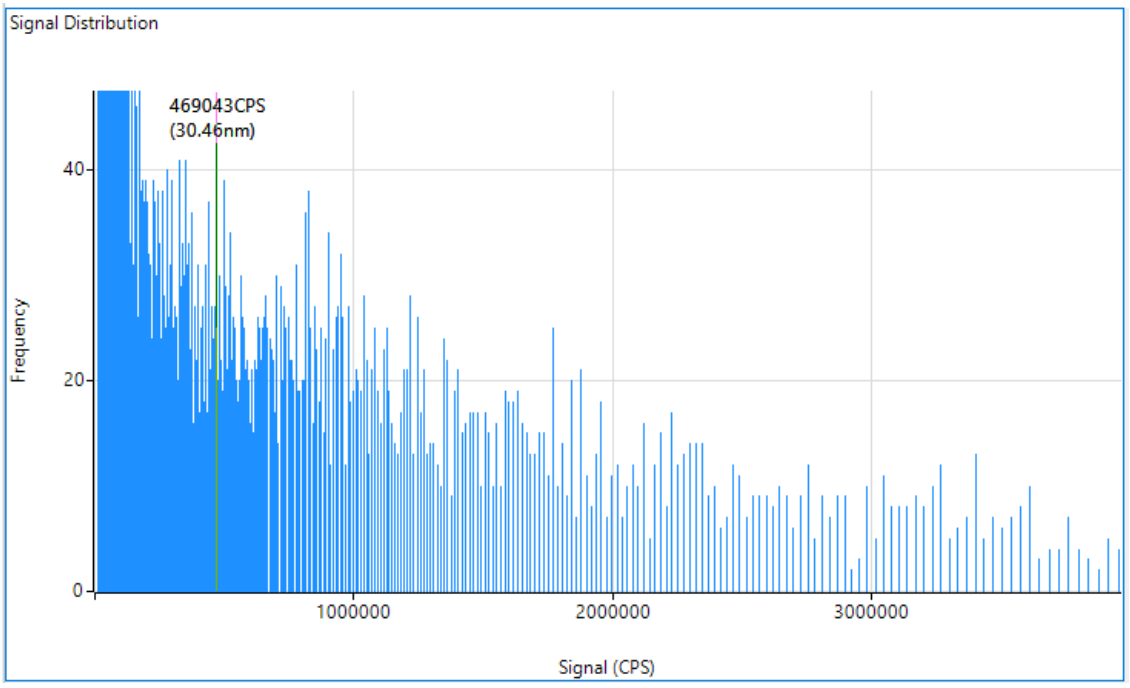

Attachment 2

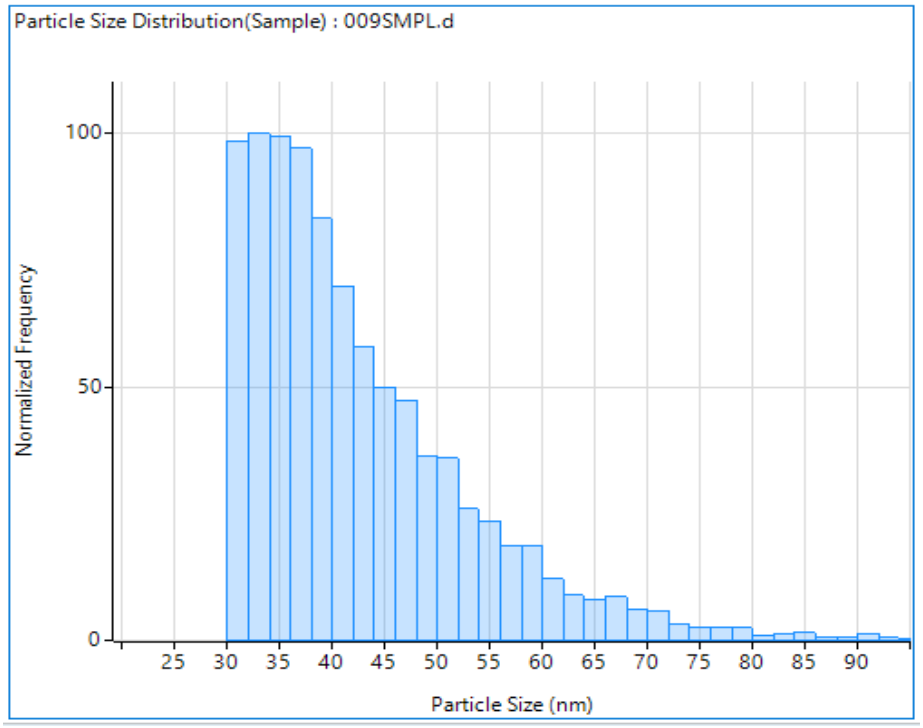

Attachment 3